JEM

Article

The Cdx2 homeobox gene suppresses intestinal tumorigenesis through non–cell-autonomous mechanisms

Camille Balbinot,[1] Olivier Armant,[2] Nabila Elarouci,[3] Laetitia Marisa,[3] Elisabeth Martin,[1] Etienne De Clara,[1] Alina Onea,[4] Jacqueline Deschamps,[5] Felix Beck,[6] Jean-Noël Freund,[1] and Isabelle Duluc[1]

[1]Université de Strasbourg, Institut National de la Santé et de la Recherche Médicale, IRFAC UMR-S1113, Fédération de Médecine Translationnelle de Strasbourg, Strasbourg, France
[2]Karlsruhe Institute of Technology, Institute of Toxicology and Genetics, Karlsruhe, Germany
[3]Cartes d'Identité des Tumeurs Program, Ligue Nationale Contre le Cancer, Paris, France
[4]Département de Pathologie, Centre Hospitalier Universitaire de Strasbourg, Strasbourg, France
[5]Developmental Biology and Stem Cell Research, Hubrecht Institute, Utrecht, Netherlands
[6]Barts and The London School of Medicine and Dentistry, London, England, UK

Developmental genes contribute to cancer, as reported for the homeobox gene *Cdx2* playing a tumor suppressor role in the gut. In this study, we show that human colon cancers exhibiting the highest reduction in *CDX2* expression belong to the serrated subtype with the worst evolution. In mice, mosaic knockout of *Cdx2* in the adult intestinal epithelium induces the formation of imperfect gastric-type metaplastic lesions. The metaplastic knockout cells do not spontaneously become tumorigenic. However, they induce profound modifications of the microenvironment that facilitate the tumorigenic evolution of adjacent *Cdx2*-intact tumor-prone cells at the surface of the lesions through NF-κB activation, induction of inducible nitric oxide synthase, and stochastic loss of function of *Apc*. This study presents a novel paradigm in that metaplastic cells, generally considered as precancerous, can induce tumorigenesis from neighboring nonmetaplastic cells without themselves becoming cancerous. It unveils the novel property of non–cell-autonomous tumor suppressor gene for the *Cdx2* gene in the gut.

INTRODUCTION

Embryonic development and tumor growth share several features. For instance, homeobox genes, which are crucial for body plan organization, can also be involved in tumorigenesis either as tumor suppressors or as oncogenes. In line with this, it is now well established that tumors represent cellular masses that are structurally organized but anatomically and functionally abnormal compared with healthy organs (Egeblad et al., 2010). Tumor growth is driven by the intrinsic properties of the cells and by cell interactions with their environment. The role of cell interactions between tumor cells and other cell types, such as cancer-associated fibroblasts, immune cells, or endothelial cells, has been widely described (Lujambio et al., 2013; Marusyk et al., 2014). However, much less is known about whether and how epithelial cells at different premalignant stages can interact and participate in tumor initiation.

Besides its role in embryonic development, the homeobox gene *Cdx2* is an important regulator of the dynamic homeostasis of the gut, providing tissue identity to the stem cells and coordinating cell proliferation and differentiation during the constant renewal of the epithelium (Verzi et al., 2011; Stringer et al., 2012; Simmini et al., 2014). Its expression is frequently altered in human colorectal cancers (CRCs) and in animal models of intestinal cancers, and convergent studies in mice have established its tumor suppressor role in the gut (Aoki et al., 2003; Bonhomme et al., 2003; Gross et al., 2008; Hryniuk et al., 2014). Recently, a functional link between B-Raf activation and loss of *Cdx2* in a subset of CRCs has demonstrated the relevance of the combination of these molecular events within tumor cells and the importance of cell differentiation dictated by *Cdx2* against intestinal tumorigenesis (Sakamoto et al., 2017; Tong et al., 2017). In the present study, starting from data obtained in a collection of human CRCs, we developed an original mouse model with the goal of uncovering the importance of indirect interactions between different types of epithelial cells at premalignant stages in triggering tumorigenesis. The results highlight a novel property of *Cdx2* in the gut, in that this homeobox gene exerts a non–cell-autonomous tumor suppressor activity. In addition, a new paradigm for metaplasia emerges, in the sense that metaplastic cells, widely considered as precancerous, can induce the tumorigenic evolution of adjacent nonmetaplastic cells without themselves becoming cancerous.

Correspondence to Jean-Noël Freund: jean-noel.freund@inserm.fr

O. Armant's present address is Institut de Radioprotection et de Sûreté Nucléaire (IRSN), PRP-ENV/SERIS/LECO, Cadarache, Saint-Paul-lez-Durance, France.

The Rockefeller University Press
J. Exp. Med. 2018 Vol. 215 No. 3 911–926
https://doi.org/10.1084/jem.20170934

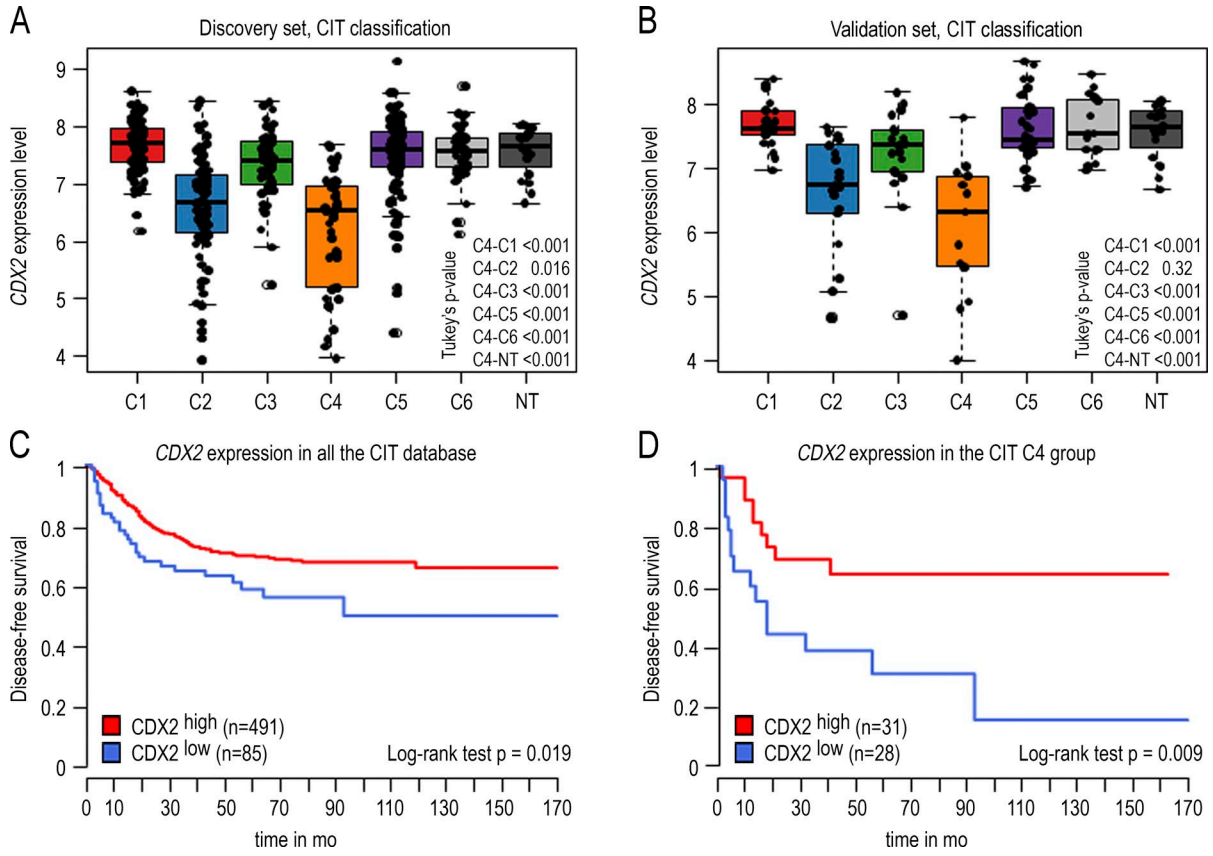

Figure 1. ***CDX2* gene expression level in 566 human colon cancers and 19 nontumoral samples of the GSE39582 dataset. (A)** Boxplot of the level of *CDX2* expression in the 443 CRC samples of the discovery set organized in the six subtypes according to Marisa et al. (2013) (C1–C6). **(B)** Boxplot of the *CDX2* expression level in the 123 samples of the validation set organized in six subtypes. Data are given ± SD. **(C)** Disease-free survival comparing $CDX2^{high}$ versus $CDX2^{low}$ CRC in the GSE39582 dataset. The cutoff for low versus high *CDX2* expression is fixed at the median of the C4 group. $CDX2^{low}$ patients exhibit a significantly reduced disease-free survival ($P < 0.019$). **(D)** Disease-free survival comparing $CDX2^{high}$ versus $CDX2^{low}$ CRC in the C4 subtype. $CDX2^{low}$ patients exhibit a significantly reduced disease-free survival ($P = 0.009$). P-values were calculated with the log-rank test.

RESULTS

Human serrated-type colon cancers with a stem cell signature exhibit a strong reduction of CDX2

Analyzing the expression of the *CDX2* homeobox gene in a cohort of 566 human CRCs (Cartes d'Identité des Tumeurs study) previously classified into six subtypes (Marisa et al., 2013) revealed a down-regulation in two subtypes: the C2 subtype, enriched with microsatellite instable and hypermutated tumors, and a stronger down-regulation in the C4 subtype characterized by serrated precursor neoplasia, stroma infiltration, and a stem cell–like/mesenchymal signature (Fig. 1, A and B). In the consensus classification system (Guinney et al., 2015), the same down-regulation was also observed in subtypes CMS1 and CMS4, including the C2 and C4 subtypes from Marisa et al. (2013) (Fig. S1). Using an unsupervised approach fixing the threshold at the median value of *CDX2* in the C4 subtype, patients of the whole cohort below the threshold exhibited worse disease-free survival (Fig. 1 C). Within the C4 subtype, disease-free survival was even worse in patients below the threshold compared with patients above the threshold (Fig. 1 D). Thus, the strong reduction of *CDX2* correlates with poor evolution of the disease.

Loss of function of *Cdx2* in the mouse intestine induces imperfect gastric-type metaplastic lesions in the cecum, which do not spontaneously undergo cancerous evolution

To address the pathological relevance of the loss of expression of *Cdx2*, mosaic gene knockout was induced in the gut epithelium of adult $AhCre^{ERT}::Cdx2^{f/f}$ mice, as described previously (Stringer et al., 2012). Mosaic knockout is mandatory for the current long-term studies because massive loss of function of *Cdx2* is lethal as a result of digestive problems (Verzi et al., 2011). Within 4–6 wk after gene knockout by β-naphthoflavone and tamoxifen (βNF+Tam) administration, the $AhCre^{ERT}::Cdx2^{f/f}$ mice exhibited subsurface cysts throughout the small intestine that did not evolve with time, as previously reported (Stringer et al., 2012). In addition, after 4 mo, all the mice analyzed in this study ($n > 25$) developed one to two polypoid lesions in the cecum, and in 20% of the mice, lesions were also found in the very distal ileum and

proximal colon (Fig. 2 A). These lesions did not compromise the life span of the animals (see Fig. 5 A). As shown in Fig. 2 (A and B), the lesions consisted of *Cdx2*-devoid glands intermingled with few *Cdx2*-intact glands, reflecting the mosaic ablation of the gene. They were covered by a single-layered polarized epithelium with local erosion in surface and exhibited signs of inflammation, with the presence of eosinophils and neutrophils in the stroma. Histologically, the lesions consisted of fundic-type glandular structures with dilated cysts together with areas of foveolar hyperplasia and antral-type glands covered by a polarized epithelium with nuclei regularly distributed at the cell base. They shared histological properties with glandular cystic and hyperplastic polyps reported in the human stomach but differed from typical hyperplastic polyps of the intestine. By immunohistochemistry (Fig. 2 C), the cecal lesions showed a loss of expression of intestinal proteins known to be downstream targets of Cdx2, such as the orthologous homeoprotein Cdx1 and the mucin Muc2, and conversely the onset of expression of gastric proteins including Claudin-18, Tff1, and Tff2. However, unlike the cecal foregut-type heteroplasia already developing during embryogenesis in heterozygous $Cdx2^{+/-}$ mice (Beck et al., 1999; Stringer et al., 2008), the lesions of $AhCre^{ERT}::Cdx2^{f/f}$ mice failed to express Sox2. To further characterize them at the molecular level, we determined their transcriptomic profile and compared it with normal cecum and stomach and also with cecal foregut-type heteroplasia developing in $Cdx2^{+/-}$ mice. This led to identification of a large number of genes (5,915) altered in the lesions of $AhCre^{ERT}::Cdx2^{f/f}$ mice compared with normal cecum (Table S1, sheet 1). The large number of genes is consistent with the Cdx2 protein being a major regulator of intestinal homeostasis and with its binding to ∼14,000 chromatin sites across the genome of enterocytes (Verzi et al., 2010). Among them, transcripts for intestinal markers were strongly reduced (i.e., Alpi, Muc3/13, Cdh17, Cdhr2/5, Fabp2, Slc51a/b, Cdx1, and Isx), whereas those for several gastric markers were turned on (i.e., Cldn18, Ctse, Gkn1/2/3, Muc1/6, Ptprn2, Tff1/2, Vsig1, Gsdma2, Krt23, Fxyd3, and Foxq1; Fig. 2 D; and Table S1, sheet 2). Yet the lesions of adult $AhCre^{ERT}::Cdx2^{f/f}$ mice exhibited a lower and more heterogeneous expression of gastric genes compared with normal stomach and also with the foregut-type heteroplasia of $Cdx2^{+/-}$ mice; moreover, several typical markers even failed to turn on (Fig. 2 D). Thus, we concluded that in the long term, the loss of *Cdx2* produces cecal lesions characterized by an imperfect gastric-type metaplastic phenotype.

Because metaplastic lesions are commonly considered to be precancerous in many organs, we questioned the pathological significance of the cecal lesions developing in $AhCre^{ERT}::Cdx2^{f/f}$ mice. In these lesions, gene ontology terms related to cancer, neoplasia, cell transformation, cell proliferation, cell survival, and growth of tumors were enriched, whereas those for apoptosis and cell death of tumor cells were underrepresented (Fig. 3 A). However, the pathohistological examination failed to display any dysplastic structure. Ki67 immunostaining revealed an important number of proliferating cells unevenly distributed predominantly in the middle third of the lesions, which is reminiscent of the localization of proliferating cells in the isthmus of the gastric mucosa, unlike the crypts in the intestine (Fig. 3 B). The canonical Wnt pathway was not abnormally activated, as indicated by β-catenin remaining associated with the plasma membranes without cytoplasmic/nuclear translocation (Fig. 3 B). However, the formation of the lesions strongly impacted the stem cell compartment, as suggested by the altered expression, either up or down, of ∼45% (173/384) of the genes of the intestinal stem cell signature (Muñoz et al., 2012; Table S1, sheet 3). For instance, the RNA sequencing data showed a strong stimulation of Sox9 (6×) and Olfm4 (>200×). This prompted us to analyze the tissue distribution of the corresponding proteins (Fig. 3, B and C). The Sox9 protein, present at the bottom of the glands in the normal stomach and at the crypt base all along the gut, was strongly expressed in both *Cdx2*-depleted glands of the lesions and in the few embedded *Cdx2*-intact glands, and also heterogeneously in the surface epithelium of the lesions. The Olfm4 protein, present in the stem/progenitor cells of the small intestine but in neither the mouse stomach nor in the cecum and colon (except for low expression in rare glands/crypts), became strongly expressed in the *Cdx2*-depleted glands of the lesions, but it was not turned on in either the embedded *Cdx2*-intact glands or in the surface epithelium. Interestingly, although the Sox9 pattern was similar in the lesions of $AhCre^{ERT}::Cdx2^{f/f}$ mice and in the foregut-type heteroplasia of $Cdx2^{+/-}$ mice, the Olfm4 pattern was very different because this protein was almost absent in the heteroplasia, with the exception of few clusters of glands histologically indistinguishable from the Olfm4-negative glands (Fig. 4 A).

The patterns obtained in the cecal lesions of $AhCre^{ERT}::Cdx2^{f/f}$ mice were compared with those observed in human lesions (Fig. 4 B). In human gastric hyperplastic polyps, the expression of Sox9 and Olfm4 was strong in more than half of the glandular structures. In contrast, in gastric-type heterotopia of the duodenum, strong Olfm4 was observed in only few glands (<10%). Finally, Meckel diverticula with gastric-type differentiation showed only rare structures expressing Sox9 at a low level, and no expression of Olfm4. All these human lesions failed to express Cdx2. These data are consistent with the notion that the imperfect gastric-type metaplastic lesions arising in the cecum of $AhCre^{ERT}::Cdx2^{f/f}$ mice share properties with human gastric hyperplastic polyps.

Based on the high level of cell proliferation and the perturbation of the stem cell compartment in the cecal lesions of $AhCre^{ERT}::Cdx2^{f/f}$ mice, a series of five animals were maintained alive up to 23–24 mo (20–21 mo after *Cdx2* knockout) to investigate whether these lesions underwent spontaneous cancerous evolution in aged animals. Pathohistological examination revealed neither dysplastic nor neoplastic structures. At the molecular level, β-catenin remained membranous without any evidence of cytoplasmic/nuclear trans-

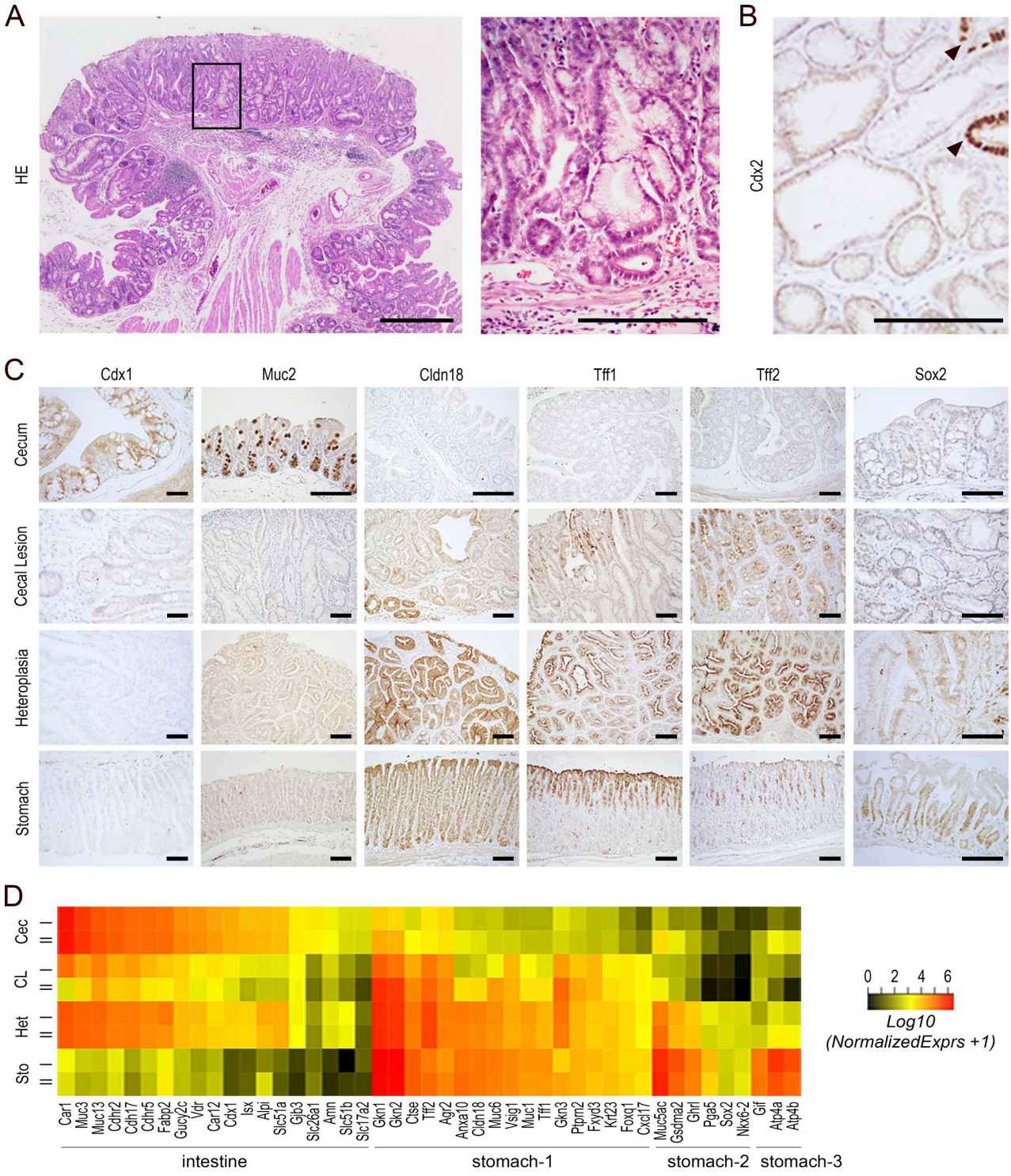

Figure 2. **Cecal lesion induced by mosaic gene knockout of *Cdx2* in the adult gut epithelium. (A)** Histology of cecal lesions in *AhCre*^{ERT}*::Cdx2*$^{f/f}$ mice 4 mo after βNF+Tam administration. Bar, 500 µm. The boxed region is magnified in the right panel. Bar, 250 µm. **(B)** Immunodetection of the Cdx2 protein. The protein is almost absent, except in few glands with intact Cdx2 (arrowheads) entrapped in the lesions. Bar, 100 µm. In A and B, $n = 20$ mice from five crossings. **(C)** Immunodetection of intestinal proteins (Cdx1, Muc2) and gastric proteins (Cldn18, Tff1, Tff2, Sox2) in the cecum of wild-type mice, cecal lesions of *AhCre*^{ERT}*::Cdx2*$^{f/f}$ mice, cecal heteroplasia of *Cdx2*$^{+/-}$ mice, and the stomach of wild-type mice. $n = 4$ animals per genotype from two crossings. Bars, 100 µm. **(D)** Heatmap comparison of transcriptomic data for intestinal and gastric genes in the cecum of wild-type mice (Cec), cecal lesions of *AhCre*^{ERT}*::Cdx2*$^{f/f}$ mice (CL), cecal heteroplasia of *Cdx2*$^{+/-}$ mice (Het), and the stomach of wild-type mice (Sto). Stomach-1 represents gastric genes up-regulated in CL and Het compared with Cec; Stomach-2 represents gastric genes up-regulated in Het but not in CL; Stomach-3 represents gastric genes up-regulated in neither CL nor in Het.

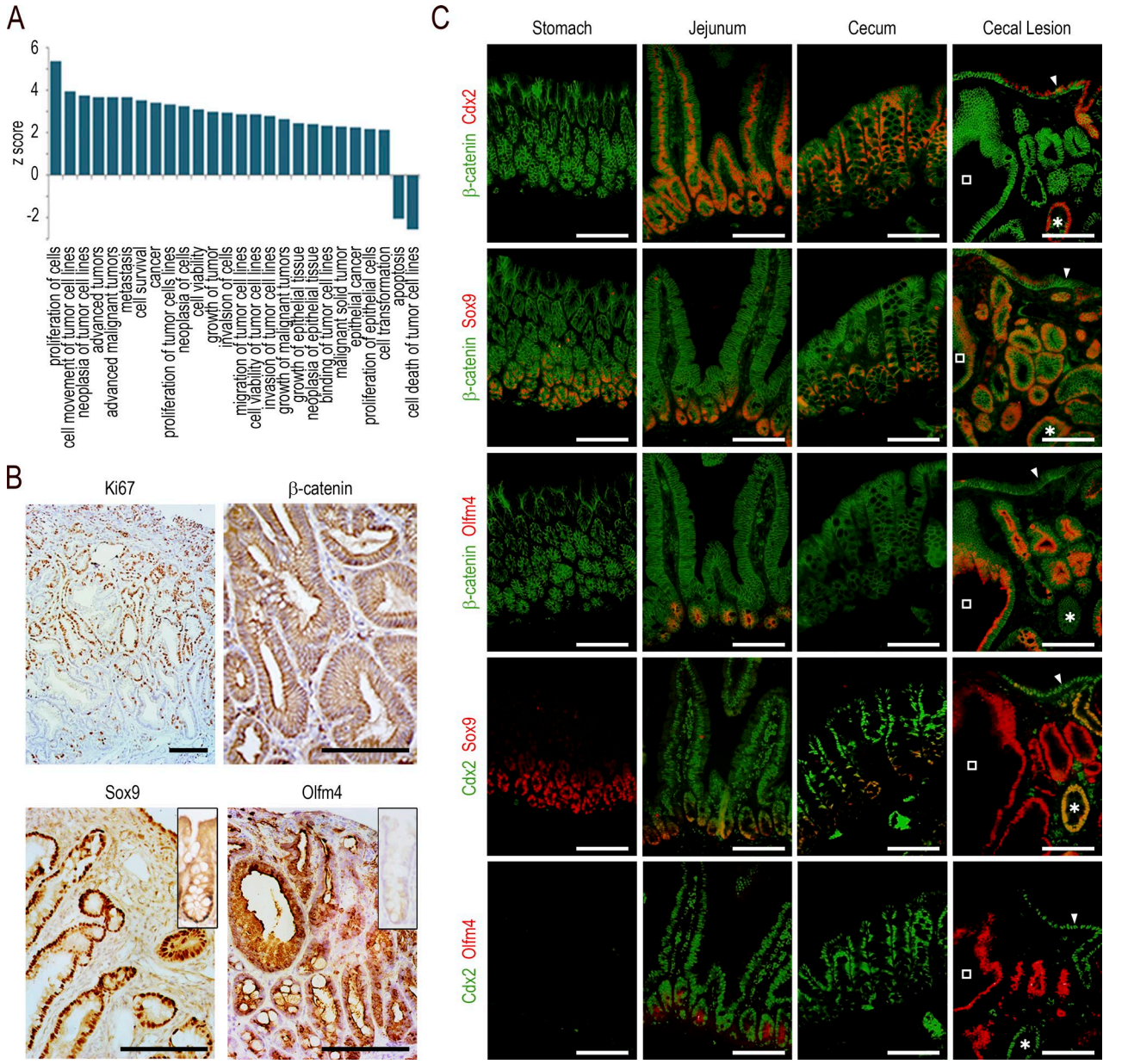

Figure 3. **Functional characterization of the cecal lesions. (A)** Gene ontology enrichment analysis for terms related to cancer in the transcriptome of the cecal lesions of *AhCre^{ERT}::Cdx2$^{f/f}$* mice compared with the cecum of wild-type mice. **(B)** Immunohistochemical staining of Ki67, β-catenin, Sox9, and Olfm4 in the cecal lesions; the insets respectively represent the Sox9 and Olfm4 patterns in wild-type cecal glands. Bars: (β-catenin) 100 µm; (Ki67, Sox9, and Olfm4) 200 µm. **(C)** Coimmunofluorescence detection of β-catenin and Cdx2, β-catenin and Sox9, β-catenin and Olfm4, Cdx2 and Sox9, and Cdx2 and Olfm4 in serial sections of the stomach, jejunum, and cecum of wild-type mice and in the cecal lesions of *AhCre^{ERT}::Cdx2$^{f/f}$* mice. In the cecal lesions, open squares show a gland depleted in Cdx2, and asterisks show a gland with intact Cdx2. The arrowheads point to the surface epithelium expressing Cdx2. Bars, 50 µm. Pictures in B and C are representative of the data obtained in $n = 4$ animals per genotype in two crossings.

location (unpublished data). Thus, in >30 *AhCre^{ERT}::Cdx2$^{f/f}$* mice analyzed at various time points, none of the cecal lesions spontaneously underwent tumorigenic evolution.

Evolution of the cecal lesions in a tumor-prone context

Based on these observations, the lesions were explored in a cancer-prone context by crossing *AhCre^{ERT}::Cdx2$^{f/f}$* mice with *Apc$^{+/\Delta 14}$* mice (Colnot et al., 2004). *Apc$^{+/\Delta 14}$* mice develop adenomatous polyps predominantly in the small intestine, but also a few in the colon and rarely in the cecum (respectively 18 ± 7 and 1 ± 1 polyps in the small intestine and in the colon per mouse, and only 1 polyp every 10 mice in the cecum). As previously reported (Colnot et al., 2004), the life span of *Apc$^{+/\Delta 14}$* animals was compromised compared with wild-type

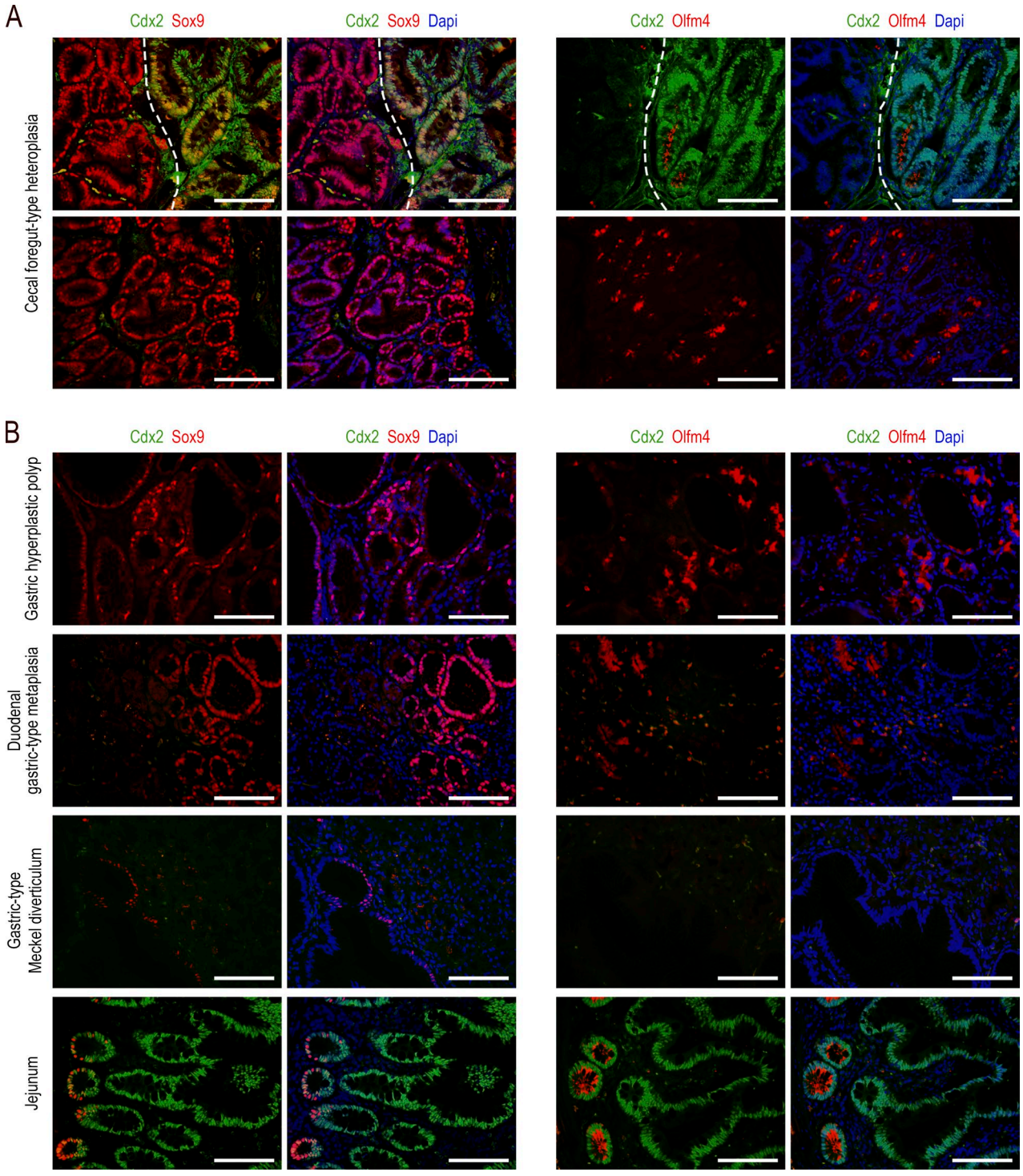

Figure 4. **Comparative expression patterns of the Cdx2, Sox9, and Olfm4 proteins in gastrointestinal lesions. (A)** Foregut-type heteroplasia in the cecum of *Cdx2*$^{+/-}$ mice. Top: region at the border (dotted line) between the normal cecal mucosa (right side) and the heteroplastic tissue (left side). The normal epithelium expresses Cdx2, whereas Sox9 and Olfm4 are present at the bottom of the glands; the heteroplastic tissue, devoid of Cdx2, shows a strong expression of Sox9 but no expression of Olfm4. Bottom: rare clusters of glands in the heteroplasia expressing both Sox9 and Olfm4. Bars, 50 µm. $n = 4$ mice. **(B)** Human lesions: hyperplastic polyp in the stomach ($n = 3$); gastric-type metaplastic polyp in the duodenum ($n = 1$); and Meckel diverticulum with gastric-type differentiation ($n = 3$). For the normal small intestinal mucosa (bottom), the crypt-villous axis is from left to right ($n = 3$). Bars, 50 µm.

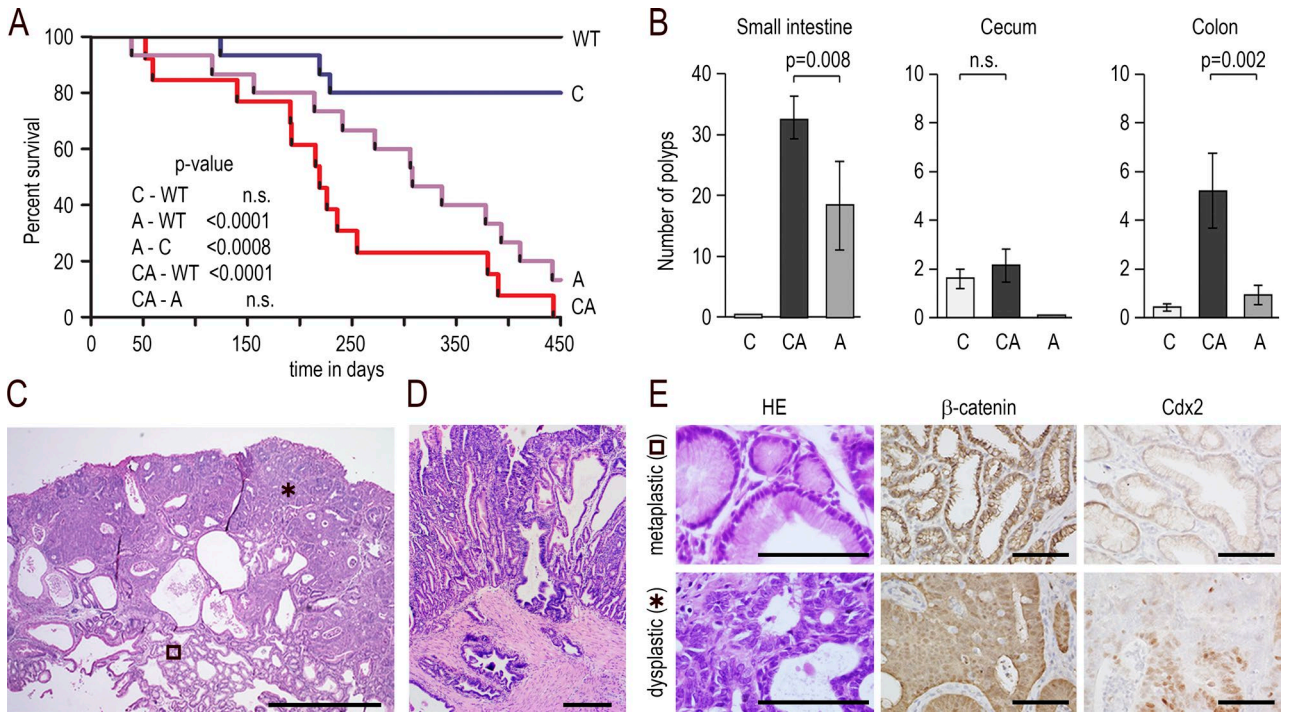

Figure 5. **Mixed tumors developing by mosaic loss of *Cdx2* combined with *Apc* heterozygosity. (A)** Survival curve (Kaplan–Meier representation) of wild-type (WT), $AhCre^{ERT}::Cdx2^{f/f}$ (C), $Apc^{+/\Delta 14}$ (A), and $Apc^{+/\Delta 14}::AhCre^{ERT}::Cdx2^{f/f}$ (CA) mice; n = 15 animals of each genotype; p-values were calculated using the log-rank test; n.s., not significant. **(B)** Number of polyps in the small intestine, cecum, and colon of $AhCre^{ERT}::Cdx2^{f/f}$ (C), $Apc^{+/\Delta 14}::AhCre^{ERT}::Cdx2^{f/f}$ (CA), and $Apc^{+/\Delta 14}$ (A) mice; n = 10 mice of each genotype; data are given ± SD; p-values were calculated using the Wilcoxon–Mann–Whitney test; n.s., not significant. **(C)** Histology of a cecal mixed tumor in $Apc^{+/\Delta 14}::AhCre^{ERT}::Cdx2^{f/f}$ mice with the juxtaposition of metaplastic-type (open square) and dysplastic areas (asterisk). Bar, 500 µm; n = 15 mice in three crossings. **(D)** Invasion beyond the muscularis mucosae. Bar, 100 µm. **(E)** Histology and immunostaining of β-catenin and Cdx2 in the metaplastic-type and dysplastic areas. Bars, 50 µm; n = 15 mice in three crossings.

mice and thus also compared with βNF+Tam-injected $AhCre^{ERT}::Cdx2^{f/f}$ mice; in the cancer-prone context, the $Apc^{+/\Delta 14}::AhCre^{ERT}::Cdx2^{f/f}$ mice treated with βNF+Tam showed a tendency to an even shorter life span, although this was not significantly different from $Apc^{+/\Delta 14}$ mice (Fig. 5 A). The $Apc^{+/\Delta 14}::AhCre^{ERT}::Cdx2^{f/f}$ mice examined 6–8 mo after βNF+Tam administration exhibited polyps in the cecum in numbers similar to the cecal lesions of $AhCre^{ERT}::Cdx2^{f/f}$ mice (one to two polyps per mouse); however, polyps were nearly two times more abundant in the small intestine (32 ± 4 vs. 18 ± 7) and five times more abundant in the colon (5 ± 2 vs. 1 ± 1) compared with $Apc^{+/\Delta 14}$ mice (Fig. 5 B). Within the whole population of mice carrying the $Ap^{\Delta 14}$ allele, we also observed rectal prolapses in higher proportion in $Apc^{+/\Delta 14}::AhCre^{ERT}::Cdx2^{f/f}$ mice (31.6%) than in $Apc^{+/\Delta 14}$ mice (21.0%). The higher incidence of rectal prolapses in these animals could relate to their tendency for a reduced life span.

Histologically, all the polyps (100%) present in the cecum of the $Apc^{+/\Delta 14}::AhCre^{ERT}::Cdx2^{f/f}$ mice showed the same typical mixed structure characterized by the juxtaposition of areas resembling the imperfect gastric-type metaplastic lesions of $AhCre^{ERT}::Cdx2^{f/f}$ mice, with cell nuclei regularly arranged at the basal side of the polarized glandular epithelium, and areas like the adenomatous polyps of $Apc^{+/\Delta 14}$ mice exhibiting tight dysplastic glands with an altered architecture, necrotic figures, cell polarity perturbations, and large hyperchromatic nuclei irregularly localized in the cells (Fig. 5, C and E). Thus, these polyps are referred to hereafter as mixed tumors. As in the cecum, all (100%) of the polyps present in the colon of $Apc^{+/\Delta 14}::AhCre^{ERT}::Cdx2^{f/f}$ mice corresponded to mixed tumors; in the small intestine, 73% of the polyps were mixed tumors, whereas the remaining 27% corresponded to typical adenomatous polyps without gastric-type metaplastic structure. Evidence for invasion beyond the muscularis mucosae was observed in 15/55 mixed tumors of $Apc^{+/\Delta 14}::AhCre^{ERT}::Cdx2^{f/f}$ mice, which indicated adenocarcinomatous evolution (Fig. 5 D). Yet this is of the same order of magnitude as observed for the polyps of $Apc^{+/\Delta 14}$ mice (12/45). By immunohistochemistry, β-catenin showed membranous distribution in the areas resembling the metaplastic lesions of $AhCre^{ERT}::Cdx2^{f/f}$ mice, but it shifted to a diffuse cytoplasmic/nuclear pattern in the areas looking like the $Apc^{+/\Delta 14}$ adenoma (Fig. 5 D). The dysplastic pictures and the altered distribution of β-catenin indicated that cells in these areas have undergone tumorigenic evolution. The mixed nature of the tumors with the juxtaposition of the

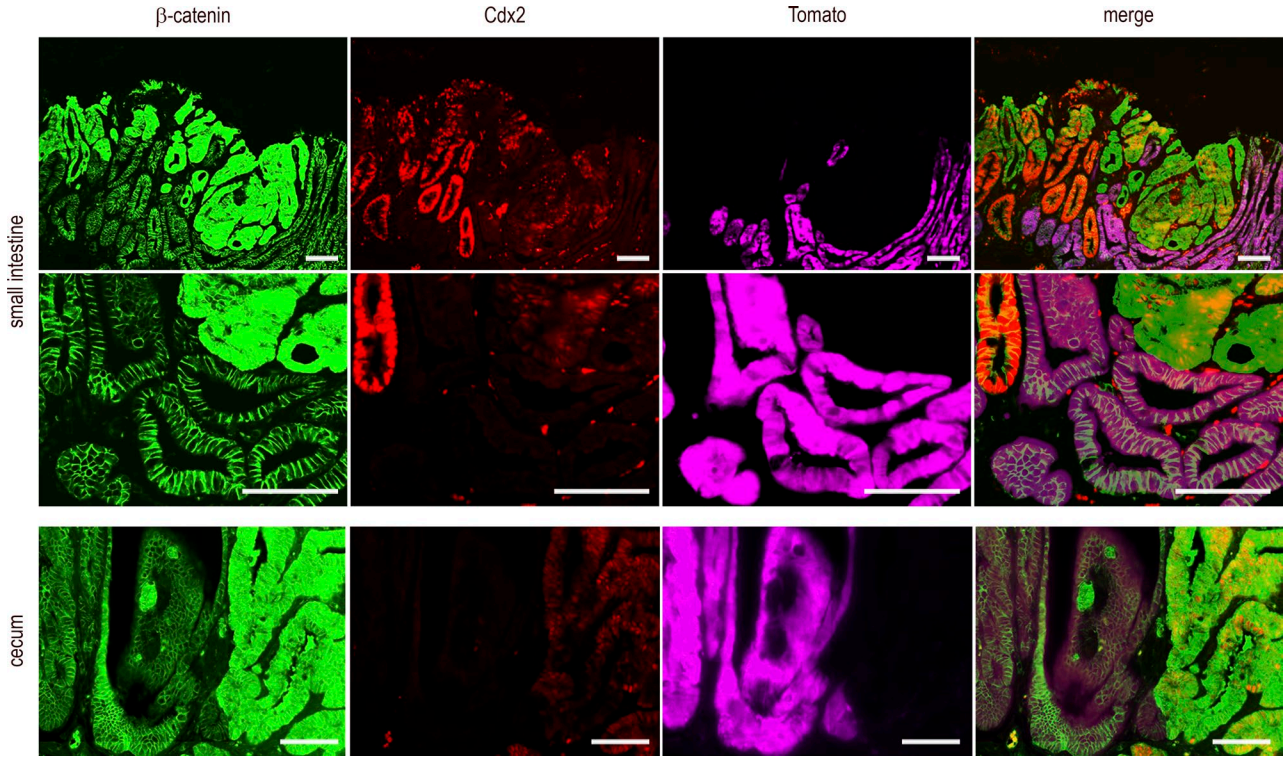

Figure 6. **Tracing of *Cdx2*-depleted cells in mixed tumors.** Detection of β-catenin, Cdx2, and Tomato in small intestinal and cecal mixed tumors of $Apc^{+/\Delta 14}$::$AhCre^{ERT}$::$Cdx2^{f/f}$::$RosaCAG^{tdTomato}$ mice. The second line of pictures represents a higher magnification of the first one. Tomato was detected by direct fluorescence emission before indirect immunodetection of β-catenin and Cdx2. The mutually exclusive patterns of Tomato and cytoplasmic/nuclear β-catenin were obtained in three mixed tumors from the cecum and three mixed tumors from the small intestine coming from four mice in two independent crossings, in four sections analyzed in each sample. Bars, 100 µm.

gastric-type metaplastic area and dysplastic areas was further confirmed by transcriptomic analyses. Indeed, Wnt pathway components were up-regulated in the cecal mixed tumors of $Apc^{+/\Delta 14}$::$AhCre^{ERT}$::$Cdx2^{f/f}$ mice compared with the lesions of $AhCre^{ERT}$::$Cdx2^{f/f}$ mice (i.e., Axin2, Cldn1, Dsc3, Fosl1, Fst, Fzd10, IL6, Lef1, Nkd1, Prox1, Tbx1, Tnfrsf19, and Wnt6), whereas gastric-type genes were turned on in the small intestinal mixed tumors compared with small intestinal dysplastic polyps of $Apc^{+/\Delta 14}$ mice (i.e., Atp4a, Car2, Ctse, Gif, Gkn1/2/3, Gsdma2, Muc1/6, Pgc, Ptprn2, Tff1/2, and Vsig1; Table S2, sheets 1 and 2). Altogether, these results indicate that the loss of *Cdx2* sensitizes the gut mucosa to tumorigenic progression in a cancer-prone context.

Non–cell-autonomous effect of *Cdx2* on intestinal tumorigenesis

Given that, on the one hand, the knockout of *Cdx2* driven by $AhCre^{ERT}$ is mosaic and that, on the other hand, tumorigenesis in $Apc^{+/\Delta 14}$ mice results from the sporadic loss of heterozygosity at the *Apc* locus (Colnot et al., 2004), the juxtaposition of metaplastic-type and dysplastic areas within the mixed tumors of $Apc^{+/\Delta 14}$::$AhCre^{ERT}$::$Cdx2^{f/f}$ mice may result either from the neoplastic conversion of metaplastic *Cdx2*-depleted cells or from detrimental interactions between adjacent cells, in that *Cdx2*-depleted cells would trigger the tumorigenic evolution of adjacent *Cdx2*-intact cells. Here, we addressed this issue using a lineage-tracing approach to follow the fate of the *Cdx2*-depleted cells. For this purpose, quadruple transgenic mice $Apc^{+/\Delta 14}$::$AhCre^{ERT}$::$Cdx2^{f/f}$::$RosaCAG^{tdTomato}$ were produced, in which activation of the Cre recombinase by βNF+Tam treatment should simultaneously disrupt the *Cdx2* gene and turn on fluorescent Tomato protein expression from the recombined $RosaCAG^{tdTomato}$ allele. Before performing this experiment, two series of controls were conducted to validate the tracing approach. First, $AhCre^{ERT}$::$Cdx2^{f/f}$::$RosaCAG^{tdTomato}$ mice were generated and used to prove the actual correlation between cells having lost *Cdx2* and cells expressing Tomato after βNF+Tam treatment (Fig. S2B). Second, $Apc^{+/\Delta 14}$::$AhCre^{ERT}$::$RosaCAG^{tdTomato}$ mice were produced, treated with βNF+Tam, and analyzed 5 mo later for fluorescence emission; the results illustrated in Fig. S2 C attest to the preservation of Tomato fluorescence in the adenomatous polyps marked by cytoplasmic/nuclear β-catenin, which conversely rules out the possibility that Tomato expression from the recombined $RosaCAG^{tdTomato}$ allele could be secondarily turned off in the dysplastic context. Having validated the tracing approach, $Apc^{+/\Delta 14}$::$AhCre^{ERT}$::$Cdx2^{f/f}$::$RosaCAG^{tdTomato}$ mice ($n = 4$) were analyzed 5 mo after βN-

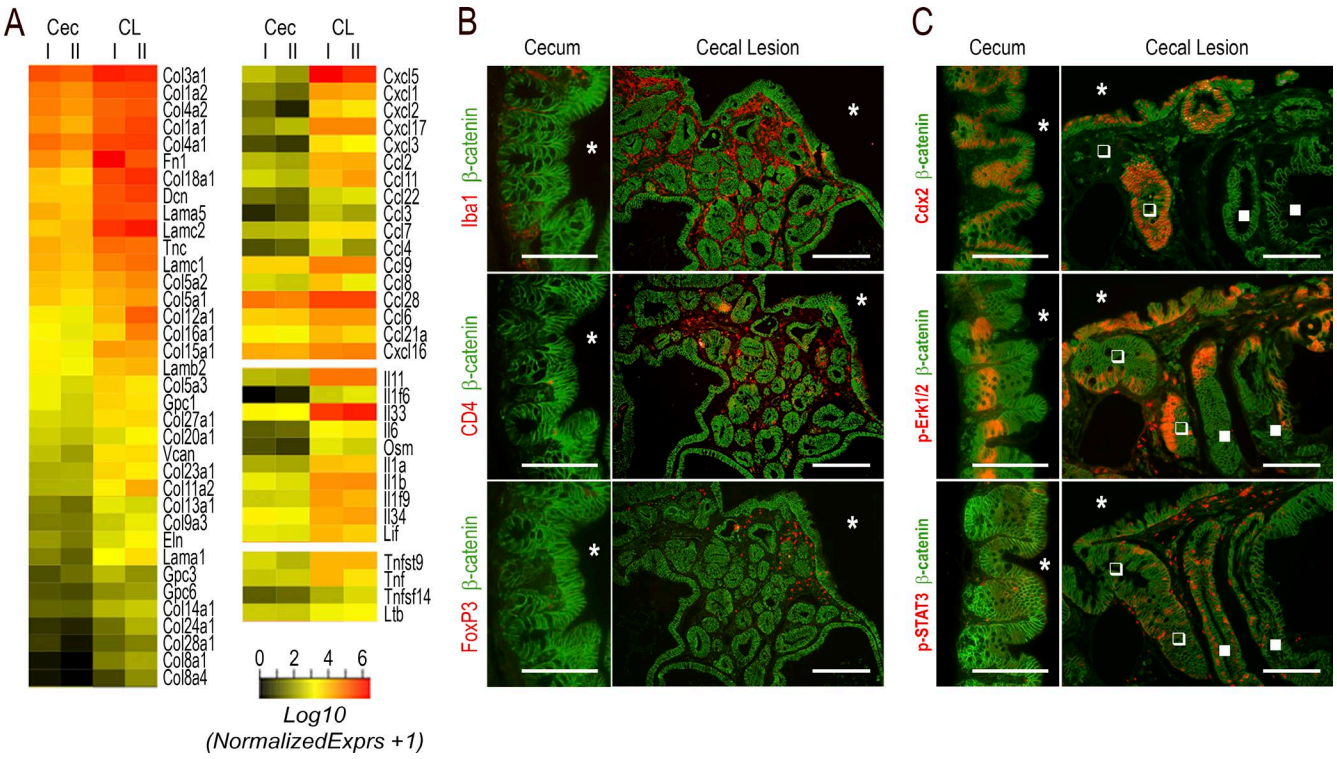

Figure 7. **Modification of the microenvironment in the cecal lesions of *AhCre^{ERT}::Cdx2$^{f/f}$* mice. (A)** Heatmap comparison of transcriptomic data for extracellular matrix genes (left) and cytokine genes (right) up-regulated in the cecal lesions of *AhCre^{ERT}::Cdx2$^{f/f}$* mice (CL) compared with the cecum of wild-type mice (Cec). **(B)** Immunodetection of Iba1$^+$ macrophages, CD4$^+$ T lymphocytes, and FoxP3$^+$ Treg lymphocytes in the normal cecal mucosa of wild-type mice and cecal lesions of *AhCre^{ERT}::Cdx2$^{f/f}$* mice. Pictures correspond to serial sections. The asterisks indicate the lumen of the cecum. Bars: (cecum) 50 µm; (cecal lesions) 100 µm. **(C)** Erk1/2 and STAT3 signaling in the cecal lesions: the immunostaining illustrates the distribution of phospho-pErk1/2 and phospho-STAT3 in the cecal lesions compared with the normal cecum. Closed and open squares respectively show *Cdx2*-depleted and *Cdx2*-intact glands. Bars: (cecum) 50 µm; (cecal lesions) 100 µm. Pictures in B and C were obtained in four mice of each genotype from two crossings.

F+Tam treatment. The results obtained in small intestinal and cecal mixed tumors (Fig. 6) led to the following conclusions: (a) cells expressing Tomato were devoid of Cdx2 and always exhibited membranous β-catenin; (b) strong and homogenous staining of Cdx2 was restricted to glands exhibiting membranous β-catenin and absence of Tomato; (c) Cdx2 was low and heterogeneous in areas with cytoplasmic/nuclear β-catenin, corresponding to cells having undergone tumorigenic evolution; and (d) dysplastic cells with cytoplasmic/nuclear β-catenin translocation never expressed Tomato. These data indicated that the cells forming the dysplastic area in the mixed tumors originated from *Cdx2*-intact instead of *Cdx2*-knockout cells. Thus, metaplastic-type *Cdx2*-depleted areas do not themselves become tumorigenic, but they create a context that stimulates tumorigenesis from adjacent *Cdx2*-intact *Apc$^{+/\Delta 14}$* tumor-prone cells. This highlights a novel property of *Cdx2* in the gut, in that this homeobox gene exerts a non–cell-autonomous tumor suppressor activity.

The loss of *Cdx2* modifies the stromal microenvironment

To investigate how *Cdx2* exerts its non–cell-autonomous tumor suppressor activity, the transcriptome of the cecal lesions of *AhCre^{ERT}::Cdx2$^{f/f}$* mice was reconsidered to identify mediators of intercellular communication (Fig. 7 A and Table S1, sheets 4 and 5). Several extracellular matrix genes potentially involved in tumor growth and progression (Lu et al., 2012) were up-regulated, as well as genes for cytokines. Among them are Tnf family members, CCL and CXCL chemokines, and interleukins. For instance, CCL2 (known to shape a tumor-permissive microenvironment; Chun et al., 2015; Zhang et al., 2015), and IL6 family members (IL6, IL11, Osm, and Lif, considered potent drivers of cancer progression; Putoczki et al., 2013) were increased, whereas IL15 and IL18 (with anticancer activity; Salcedo et al., 2010; Bahri et al., 2015) were decreased. In line with this, the cellular microenvironment was also modified, as illustrated by the widespread infiltration of macrophages and by the concentration underneath the surface epithelium of the lesions of CD4$^+$ T lymphocytes and focally of FoxP3$^+$ Treg lymphocytes (Fig. 7 B), whereas CD8$^+$ lymphocytes were barely detected.

Cytokines activate signaling pathways through mediators such as Erk, STATs, and NF-κB. Phospho-Erk1/2, present in crypt base epithelial cells in the normal cecum, shifted to an irregular pattern at the surface of the cecal lesions of

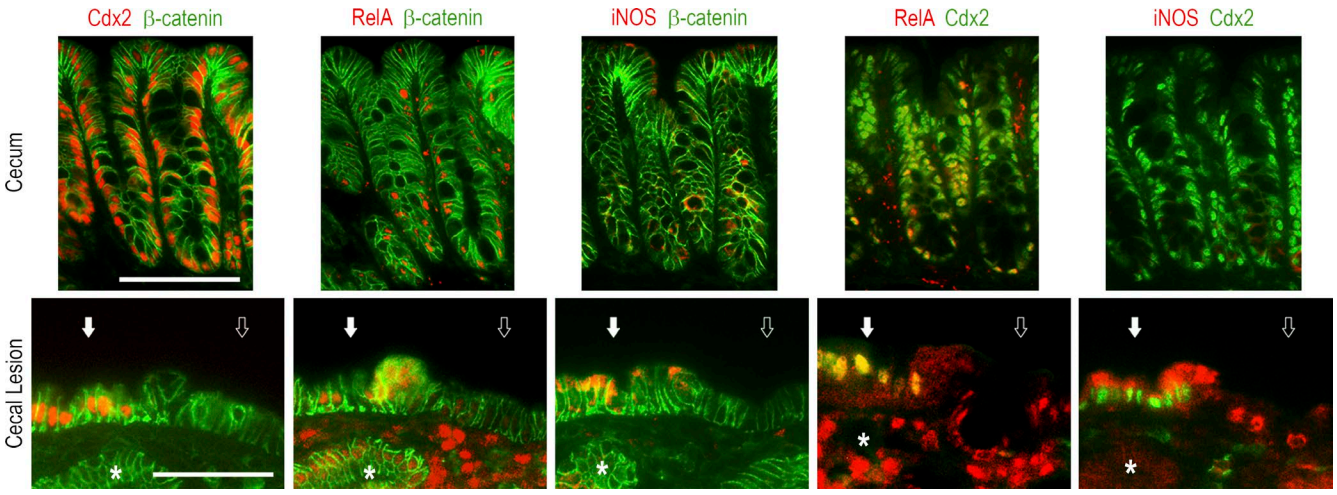

Figure 8. **NF-κB activation and iNOS induction in the cecal lesions of *AhCre^{ERT}::Cdx2$^{f/f}$* mice.** Coimmunodetection of Cdx2 and β-catenin, RelA (p65 NF-κB) and β-catenin, iNOS and β-catenin, RelA and Cdx2, and RelA and Cdx2 in the normal cecal mucosa of wild-type mice and the cecal lesions of *AhCre^{ERT}::Cdx2$^{f/f}$* mice. Open and closed arrows respectively show *Cdx2*-devoid and *Cdx2*-expressing surface epithelium. The asterisk points to a *Cdx2*-depleted gland underneath the surface epithelium. Pictures correspond to serial sections. They were obtained in four mice of each genotype from two independent crossings. Bars, 100 µm.

AhCre^{ERT}::Cdx2$^{f/f}$ mice and occasionally in subjacent glands, regardless of whether they were depleted in Cdx2 (Fig. 7 C). Phospho-STAT3 labeled infiltrating cells in the stroma of the lesions and sporadically also epithelial cells, irrespective of their Cdx2 status (Fig. 7 C). Importantly, the pattern of NF-κB was profoundly modified in the lesions (Fig. 8). Indeed, besides its presence in the nuclei of cells infiltrating the stroma, NF-κB was activated and translocated into the nucleus of epithelial cells at the surface epithelium composed of *Cdx2*-intact cells; this contrasts with the normal cecal epithelium, in which nuclear NF-κB is only weakly detected with a decreasing gradient from the bottom to the top of the crypts. This observation is particularly interesting in light of recent findings reporting that gut tumorigenesis can be initiated from non–stem cells instead of stem cells by combining the activation of Wnt and NF-κB signaling (Schwitalla et al., 2013). Moreover, the activation of the NF-κB pathway has been shown to stimulate *Apc*-dependent tumorigenesis in the gut, and this effect was related to the induction of iNOS/nos2 by NF-κB (Shaked et al., 2012). Strikingly, transcriptomic data revealed an approximately sixfold increase of iNOS/nos2 mRNA in cecal lesions compared with the normal cecum ($q < 0.0001$). In addition, this correlated not only with the infiltration of the stroma by iNOS-positive cells, but also with the focal induction of iNOS in *Cdx2*-intact cells also exhibiting nuclear NF-κB in the surface epithelium of the lesions (Fig. 8).

Surface origin and iNOS-dependent tumorigenesis in the mixed tumors

These observations prompted us to investigate whether the emergence of dysplastic areas within the mixed tumors is actually associated with *Apc* loss of heterozygosity, and whether the process is initiated at the surface of the lesions and is iNOS dependent. PCR genotyping of individual glands microdissected within cecal mixed tumors of *Apc$^{+/Δ14}$::AhCre^{ERT}::Cdx2$^{f/f}$* mice showed that the wild-type allele of *Apc* was preserved in the metaplastic-type *Cdx2*-knockout glands but lost in the dysplastic glands, as in typical *Apc$^{+/Δ14}$* adenomatous polyps (Fig. 9 A). This indicates a similar molecular mechanism of oncogenic Wnt pathway activation through *Apc* loss of heterozygosity in the dysplastic area of the mixed tumors of *Apc$^{+/Δ14}$::AhCre^{ERT}::Cdx2$^{f/f}$* mice, as in *Apc$^{+/Δ14}$* mice (Colnot et al., 2004).

Next, we addressed the site of emergence of the dysplastic area in the mixed tumors. For this purpose, the cytoplasmic/nuclear localization of β-catenin was used as a marker of the loss of *Apc*, because Colnot et al. (2004) have reported that β-catenin translocation already accompanies the loss of *Apc* in early lesions. First, we entirely cut cecal mixed tumors ($n = 3$) of *Apc$^{+/Δ14}$::AhCre^{ERT}::Cdx2$^{f/f}$* mice. This led to identification of small invaginations in the surface epithelial layer, not connected to deeper glands as assessed by serial sections analysis, which contained cells or groups of cells with cytoplasmic/nuclear β-catenin; these cells did not express Olfm4 (like normal cecum in mice) but exhibited a reduced level of Cdx2 and an increased level of Sox9 protein compared with adjacent nontransformed cells of the epithelial lining in which β-catenin remained membranous (Fig. 9 B and Fig. S3). Second, we analyzed β-catenin–immunostained sections coming from nine mixed tumors of seven *Apc$^{+/Δ14}$::AhCre^{ERT}::Cdx2$^{f/f}$* mice for the position of the dysplastic glands in the depth of the polyps. Plotting the results obtained for a total of 77 of these structures revealed

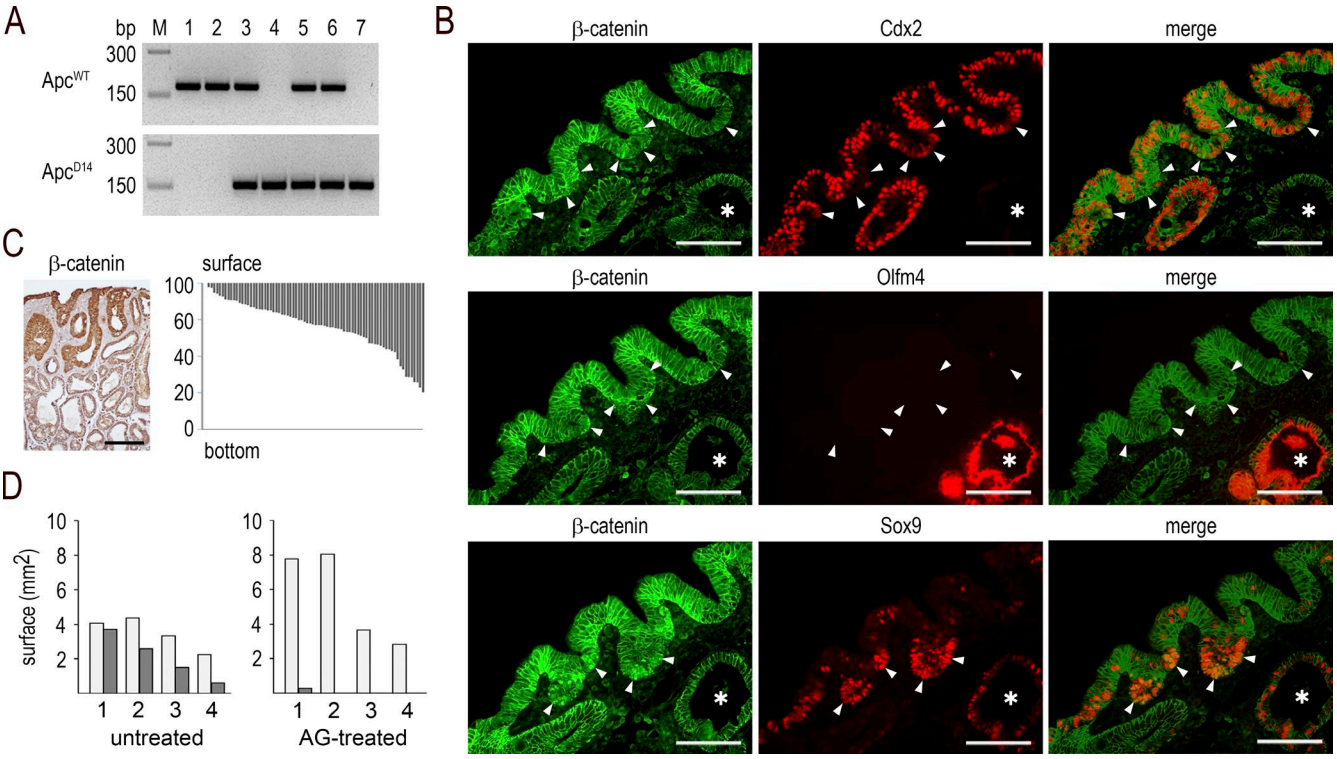

Figure 9. **Surface initiation and iNOS-dependence of the dysplastic structures in mixed tumors. (A)** Genotyping of microdissected glands for the *Apc*^{wt} and *Apc*$^{\Delta 14}$ alleles: (1) normal cecal gland and (2) *Cdx2*-depleted gland in cecal lesions of *AhCre*^{ERT}*::Cdx2*$^{f/f}$ mice; (3) normal and (4) dysplastic gland in *Apc*$^{+/\Delta 14}$ mice; (5) normal cecal gland, (6) metaplastic-type gland, and (7) dysplastic gland in mixed tumors of *Apc*$^{+/\Delta 14}$*::AhCre*^{ERT}*::Cdx2*$^{f/f}$ mice. PCR results are representative of the results obtained in $n = 3$ mice. **(B)** Immunodetection of β-catenin, Cdx2, Olfm4, and Sox9 in the *Cdx2*-expressing surface epithelium of mixed tumors. The arrowheads point to surface epithelial cells with cytoplasmic/nuclear β-catenin; the asterisks show *Cdx2*-depleted glands. Pictures correspond to serial sections. They were obtained in $n = 10$ mice. Bars, 50 µm. **(C)** Left: localization of the dysplastic glands in mixed tumors by β-catenin immunostaining, showing cytoplasmic/nuclear accumulation in glands connected to the surface epithelium. Bar, 100 µm. Right: distribution of dysplastic glands. Each bar represents the localization and extent of one dysplastic structure along the surface-to-bottom axis of mixed tumors. Results are expressed as percentage of the height of the mixed tumors. They correspond to data obtained from nine mixed tumors in seven mice. **(D)** Surface (square millimeters) of the metaplastic-type areas (light gray) and dysplastic areas (dark gray) in the lesions developed in the cecum of *Apc*$^{+/\Delta 14}$*::AhCre*^{ERT}*::Cdx2*$^{f/f}$ mice either untreated or treated with AG. Values represent the mean surfaces in 12 sections for each sample. They were obtained from $n = 4$ AG-treated mice and $n = 4$ untreated mice.

an uneven distribution: they were all connected to or located immediately underneath the surface layer and extended more or less deeply into the tumors (Fig. 9 C). Collectively, these results suggest that the loss of heterozygosity of *Apc* occurs in the *Cdx2*-intact surface epithelial layer and that the dysplastic structures progressively cover and invade the subjacent *Cdx2*-depleted metaplastic tissue.

Finally, because the dysplastic areas are composed of *Cdx2*-intact cells and emerge from the surface of the lesion, and because the surface cells focally express iNOS, which is known to accelerate *Apc* loss and initiate tumorigenesis (Shaked et al., 2012), we investigated the involvement of iNOS in the emergence of dysplasia in *Apc*$^{+/\Delta 14}$*::AhCre*^{ERT}*::Cdx2*$^{f/f}$ mice. For this purpose, animals were treated with βNF+Tam and, 2 wk later, given the iNOS inhibitor aminoguanidine (AG) *ad libitum* in drinking water for 3 mo. Sections of the lesions developing in the cecum of these mice were analyzed histologically and by immunostaining for Cdx2 and β-catenin to identify and record the metaplastic-type area and dysplastic areas. As illustrated in Fig. 9 D, three of the four cecal lesions analyzed in AG-treated mice showed no dysplastic area, and the fourth lesion exhibited only a small area of this type of structure; this contrasted with the higher proportion of dysplastic areas observed in every cecal mixed tumor of untreated mice. In parallel, we observed that the AG treatment reduced the tumor load in the small intestine (10 ± 3 vs. 28 ± 4) and colon (2 ± 1 vs. 5 ± 2) of these *Apc*$^{+/\Delta 14}$*::AhCre*^{ERT}*::Cdx2*$^{f/f}$ mice compared with untreated mice, whereas it had no significant effect in *Apc*$^{+/\Delta 14}$ mice (13 ± 6 vs. 14 ± 3 tumors in the small intestine and 1 ± 1 vs. 0 in the colon). These results suggest that iNOS actually contributes to the emergence of dysplasia in the context of the *Apc*$^{+/\Delta 14}$*::AhCre*^{ERT}*::Cdx2*$^{f/f}$ mice; moreover, they are consistent with the data reported by Shaked et al. (2012) showing that the iNOS inhibitor AG

does not significantly hamper *Apc*-dependent tumorigenesis unless it is triggered by NF-κB/iNOS activation.

DISCUSSION

Based on clinical data showing that the strong reduction of the homeobox gene *CDX2* in human CRC correlates with poor evolution of the disease, we used a mouse model of mosaic knockout to address the long-term effect of this gene's deficiency in the gut. Although abrogating the function of *Cdx2* results in the formation of imperfect gastric-type metaplastic lesions, these lesions did not spontaneously evolve in cancer even in aged animals. This is consistent with the fact that overexpressing a dominant-negative splicing variant of *Cdx2* in the duodenum also led to the formation of lesions with gastric-type metaplastic properties without spontaneous neoplastic evolution (Balbinot et al., 2017). Nevertheless, by developing the original model that combines the mosaic knockout of *Cdx2* with the stochastic loss of function of the *Apc* tumor suppressor gene, we uncovered that functional interactions between distinct types of noncancerous epithelial cells—metaplastic-type and tumor-prone, respectively—can accelerate tumorigenesis. These deleterious interactions are indirect and involve modifications of the microenvironment driven by the metaplastic-type *Cdx2*-deficient cells that trigger chronic activation of NF-κB and induction of iNOS in *Cdx2*-intact tumor-prone cells, which subsequently undergo *Apc* loss of heterozygosity and generate dysplastic structures. Thus, this study highlights a novel and original property of *Cdx2* in the gut, in that this homeobox gene exerts non–cell-autonomous tumor suppressor activity mediated by changes in the stromal environment. Because the cecal epithelium can be the seat of adenomatous development in $Apc^{+/\Delta 14}$ mice, even at a very low rate, we believe that the environment created by the metaplastic-type *Cdx2*-depleted cells would stimulate *Apc* loss of function in the adjacent *Cdx2*-intact cells rather than bringing out latent mutations. The non–cell-autonomous tumor suppressor activity represents a new property for this homeobox gene, already reported to exhibit cell-autonomous tumor suppressor activity in the gut through its impact on many cellular and molecular functions including apoptosis, cell differentiation, cell proliferation, chromosome stability, and DNA repair (Aoki et al., 2003; Bonhomme et al., 2003; Renouf et al., 2012; Sakamoto et al., 2017; Tong et al., 2017). Only a few examples of non–cell-autonomous tumor suppressor activity have been described so far, for instance in liver and brain tumors and also in melanoma (Andoniadou et al., 2013; Lujambio et al., 2013; Mescher et al., 2017), probably because it needs to develop appropriate lineage tracing approaches. This mechanism is likely underrated despite its potential not only for tumor initiation, but also in the emergence of subclonal heterogeneity (Marusyk et al., 2014).

The findings reported here are important regarding the pathological relevance of metaplastic-type lesions displayed in a wide range of epithelial organs, including, for instance, the digestive, respiratory, and urinary tracts. Indeed, metaplasia is generally considered precancerous because of its presumptive sensitivity to progress into neoplasia. Here, we provide a novel paradigm in that metaplastic cells can also trigger tumorigenesis without themselves becoming cancerous but by inducing the cancerous evolution of adjacent nonmetaplastic cells. The reason why *Cdx2*-depleted metaplastic-type cells do not become dysplastic, unlike adjacent *Cdx2*-intact cells, is unknown. One possibility is related to the fact that that these cells show a strong induction of Sox9 and Olfm4, which have been reported to antagonize tumorigenesis (Bastide et al., 2007; Liu et al., 2016; Prévostel et al., 2016). Also remarkable is that the tumorigenic evolution of *Cdx2*-intact cells does not occur in glands randomly embedded in the metaplastic lesions, but at the level of *Cdx2*-intact cells of the surface epithelial layer. This surface is made of patches of *Cdx2*-intact cells, *Cdx2*-depleted cells, and also eroded areas. Previous studies have shown that reducing the *Cdx2* level in mice increases intestinal permeability and sensitivity to proinflammatory treatment (Calon et al., 2007), and that *Cdx2* modulates the motility and mechanical properties of the intestinal epithelial cells (Gross et al., 2008; Platet et al., 2017). Therefore, the mosaic deletion of *Cdx2* creates a complex picture with abrasion and tissue repair from *Cdx2*-intact and *Cdx2*-deleted cells, which may contribute to the resulting modification of the underpinning stroma. The surface epithelial lining of the lesions is therefore at a critical position at the interface between the luminal content with the microbiota and the activated stroma, which may facilitate *Apc* loss of heterozygosity. The surface origin of the dysplasia represents an alternative to the model of tumor initiation in the crypt stem cells (Barker et al., 2009). It is in line with previous descriptions of top-down morphogenesis of colon cancers in humans (Shih et al., 2001) and with the mouse model of tumorigenesis initiated from dedifferentiated cells located in small intestinal villi by combining the activation of the Wnt and NF-κB pathways (Schwitalla et al., 2013).

Corroborating previous studies, our data strengthen the notion that human CRCs with a strong reduction of *CDX2* principally segregate within the subtype of serrated neoplasia with a stem cell signature (De Sousa E Melo et al., 2013; Bae et al., 2015; Dalerba et al., 2016) and also are characterized by the ectopic expression of gastric markers (Matsuda et al., 2010; Sentani et al., 2013; Kim et al., 2015). These cancers exhibit a worse evolution. Importantly, the lesions developing here after *Cdx2* loss in mice share several stromal and immune properties with the serrated subtype of human CRCs (Becht et al., 2016). These include a high expression of extracellular matrix molecules, myeloid chemokine Ccl2, complement components (C1qb, C1qc, C1ra, C1rb, C1s, C3, Cfh, and Cfi), angiogenic factors (Vegfb, Pdgfb, Pdgfc, and Pdgfd), and immunosuppressive molecules (Tgfb2, Tgfb3, Lgals1, and Lgals2). These similarities make the mice developed in this study a relevant animal model to investigate the complex modifications of the microenvironment leading to the neoplastic conversion of premalignant lesions. This is central in the perspective of the development of efficient preventive

strategies and treatments of cancer targeting the microenvironment and its interaction with tumor cells.

MATERIALS AND METHODS

Human CRC samples and analysis

The 566 transcriptomic profiles recorded in GSE39582l (Marisa et al., 2013) were analyzed. Comparison of the expression levels of *CDX2* between the C4 CRC subtype and the other subtypes was performed using independent two-group *t* test (function t.test, stats R package). CRC subtypes means comparison was performed using Tukey post hoc test after two-way ANOVA (function TukeyHSD, stats R package). Disease-free survival was defined as the time from surgery to the first recurrence. Survival curves were obtained according to the method of Kaplan and Meier (function Surv, R package survival), and differences between survival distributions were assessed by log-rank test.

Human tissue samples were obtained at the University Hospital of Strasbourg (France) according to the recommendations of the French Ethical Committee and the ethical standards of the 1964 Declaration of Helsinki. Patients provided written informed consent.

Mouse strains and treatments

Mice were used according to the protocol approved by the Committee on the Ethics of Animal Experiments of the University of Strasbourg (CREMEAS, C2EA-35) under the permit number AL/43/50/02/13. $AhCre^{ERT}$ (Ireland et al., 2004), $AhCre^{ERT}$::$Cdx2^{f/f}$ (Stringer et al., 2012), and $Apc^{+/\Delta 14}$ mice (Colnot et al., 2004) have been described. $Rosa$-$CAG^{tdTomato}$ mice (strain Ai9) were provided by the Jackson Laboratory. Strains were backcrossed at least eight times. Littermates were used as controls throughout this study.

Mice were genotyped by PCR amplification of tail DNA (Viagene, DirectPCR Lysis Reagent mouse tail; Euromedex) using the following primers: $Cdx2^{wt}$ and $Cdx2^{f}$ alleles, 5′-TGGGGCAATCTTAATGGGTA-3′ and 5′-TGTAGCCTCGACTTGGCTTT-3′; Apc^{wt} allele, 5′-CTGTTCTGCAGTATGTTATCA-3′ and 5′-CTATGAGTCAACACAGGATTA-3′; $Apc^{\Delta 14}$ allele, 5′-CTGTTCTGCAGTATGTTATCA-3′ and 5′-TATAAGGGCTAACAGTCAATA-3′; $AhCre^{ERT}$ allele, 5′-GCCTGGTCTGGACACAGTCC-3′ and 5′-GGTTCAGCATCCAACAAGGC-3′; $RosaCAG^{tdTomato}$ allele, 5′-CTGTTCCTGTACGGCATGG-3′ and 5′-GGCATTAAAGCAGCGTATCC-3′; and $Rosa^{wt}$ allele, 5′-AAGGGAGCTGCAGTGGAGTA-3′ and 5′-CCGAAAATCTGTGGGAAGTC-3′.

Mice 3 mo of age were intraperitoneally injected with 1.6 mg βNF+TAM (Sigma-Aldrich) in corn oil, once daily for 4 d. For the treatment with the iNOS inhibitor, they were injected with βNF+Tam, and 2 wk later they were given 2 g/L AG (Sigma-Aldrich) in drinking water. The pathohistological evaluation of the lesions developed in the mice used in this study was performed independently by two pathologists of the University Hospital of Strasbourg: A. Onea and M.P. Chenard.

RNA extraction and analysis by RNA sequencing

RNA was extracted from tissue fragments with Tri Reagent (Euromedex) and analyzed using nanoRNA chips on a Bioanalyser 2100 (Agilent Technologies). 1 µg of total RNA was used for the construction of the mRNA sequence libraries with Illumina's TruSeq RNA sample kit (Illumina). Poly(A) RNA was selected by two rounds on poly-dT–coated magnetic beads, followed by fragmentation and first-strand cDNA synthesis with Superscript II (Thermo Fisher Scientific) using random hexamer primers. The cDNA fragments were subjected to end repair and dA tailing, ligated to indexed bar-coded adapters, and subjected to 12 cycles of PCR. Concentration and validation of the libraries were made with DNA1000 chips loaded on a Bioanalyser 2100. Paired-end 50-bp reads were obtained with a HiSeq1000 by multiplexing three libraries on one lane. Demultiplexing and generation of raw fastq files were performed with Casava v1.7. Mapping against the reference mouse genome GRCm38 was performed with tophat 2 (Trapnell et al., 2009) using the following options: b2-sensitive, a 5, p 5, library-type, fr-unstranded, r 180, mate-std-dev 80, and exon-exon reference from Ensembl v75. Quantification of the reads was performed with HTSeq v.0.5.3p3 (Anders et al., 2015) with the following options: stranded = no, mode = union; and using the reference gene annotation from Ensembl v75. Normalization and differential expression analysis was made with DESeq2 (Love et al., 2014). Unless otherwise stated, genes with a log2(fold change [FC]) ≥1 and adjusted p-value (*q*-value) <0.01 were considered as differentially expressed. Data analysis was performed using Ingenuity Pathway Analysis (Qiagen). The transcriptomic data have been deposited in the GEO database under accession number GSE89992.

Histology and immunohistology

Tissue samples were fixed with 4% PFA and embedded in paraffin. Sections (5 µm) were deparaffinized and treated for antigen retrieval for 10 min in 10 mmol/L sodium citrate, pH 6, in a microwave oven for every primary antibody except anti-Iba1, and then blocked in 5% normal goat serum and 0.1% Triton X-100–PBS for 1 h at room temperature. Slides were incubated overnight at 4°C with primary antibodies diluted in 0.1% Triton X-100–PBS and washed in this saline buffer. Primary antibodies were as follows: mouse anti–β-catenin (clone 14; dilution 1:500; BD Transduction Lab), mouse anti-CD4 (50134-M08H; dilution 1:500; Sino Biological), goat anti-CD8b (M-20, sc-1144; dilution 1:500, Santa Cruz Biotechnology), rabbit anti-Cdx1 (Bonhomme et al., 2003; dilution 1:1,000), mouse anti-Cdx2 (CDX2-88, F/MU392A-UC; dilution 1:500; Biogenex), rabbit anti-Cdx2 (EPR2764Y, ab76541; dilution 1:10,000; Thermo Fisher Scientific), rabbit anti-Cldn18 (38-8000; dilution 1:500; Invitrogen), rat anti-FoxP3 (FJK-16s, 14-5773-80; dilution 1:500; Affymetrix eBio-

science), rabbit anti-Iba1 (orb10863; dilution 1:500; Biorbyt), rabbit anti-iNOS (M-19, sc-650; dilution 1:500; Santa Cruz Biotechnology), rabbit anti-Ki67 (RM9106-S; dilution 1:500; Thermo Fisher Scientific), rabbit anti-Muc2 (H-300, sc-15334; dilution 1:1,000; Santa Cruz Biotechnology), rabbit anti-Olfm4 (D6Y5A, mouse-specific; dilution 1:500; Cell Signaling Technology), rabbit anti-Olfm4 (ab85046, human-specific; dilution 1:500; Abcam), rabbit anti-p-Erk1/2 (D11A8, mAb5683; dilution 1:500; Cell Signaling Technology), rabbit anti–p-STAT3 (ab76315; dilution 1:500; Abcam), rabbit anti-RelA (NF-κB p65; C-20, sc-372; dilution 1:500; Santa Cruz Biotechnology), rabbit anti-Sox2 (AB5603; dilution 1:500; Millipore), rabbit anti-Sox9 (De Santa Barbara et al., 1998; dilution 1:500), rabbit anti-Tff1 (Karam et al., 2004; dilution 1:500), rabbit anti-Tff2 (Karam et al., 2004; dilution 1:500), and rat anti-Tomato (clone 16D7; dilution 1:250; KerFast). For immunohistochemical staining, secondary biotinylated antibodies (dilution 1:2,000; Vector Laboratories) were revealed using the Vectastain ABC kit (Vector Laboratories). For immunofluorescence detection, secondary goat anti-mouse antibody labeled with Alexa Fluor 488 (dilution 1:1,000; Molecular Probes) and goat anti-rabbit antibody labeled with Alexa Fluor 568 (dilution 1:1,000; Molecular Probes) were used. Sections were visualized with an Axio Zoom.V16 microscope, an Axiophot microscope, or an Axio Imager Z2 microscope (Zeiss).

For the combined detection of Tomato, β-catenin, and Cdx2 proteins in tissue sections, a two-step procedure was developed. In the first step, sections were deparaffinized and covered with 0.1% Triton X100–PBS buffer, and a picture of the direct fluorescence emitted by Tomato was taken. In the second step, the sections were treated for antigen retrieval for 10 min in 10 mmol/L sodium citrate, pH 6, in a microwave oven, which (a) destroys the direct fluorescence emission by Tomato and (b) allows further detection of β-catenin and Cdx2 by indirect immunofluorescence labeling, as described in the above paragraph. To validate this procedure, we verified that the detection of Tomato by direct fluorescence emission in deparaffinized sections was as efficient as the detection of the Tomato protein by indirect immunofluorescence in the same sections. For this purpose, cecal sections of $AhCre^{ERT}::RosaCAG^{tdTomato}$ mice treated with βNF+Tam were first processed for Tomato detection by direct fluorescence emission, and then the Tomato protein was revealed by indirect immunofluorescence using the anti-Tomato antibody. The results illustrated in Fig. S2 A demonstrate perfect superimposable patterns.

Tissue microdissection for genomic PCR analysis

Tissue sections of 10 µm fixed in 4% PFA and embedded in paraffin were sliced on FrameSlides PET Membrane slides (Leica) and stained with Harris, and serial sections were immunostained for β-catenin and Cdx2 to ascertain the identity of the microdissected glands. Areas of ∼100 cells were microdissected using an LMD 6000 laser microscope (Leica Microsystems), and genomic DNA was extracted using QIAamp DNA FFPE Tissue kit (Qiagen). Identification of the Apc^{wt} and $Apc^{\Delta 14}$ alleles was performed by PCR using the same primers as for animal genotyping.

Online supplemental material

Fig. S1 shows the results of the analysis of the transcriptomic data of the human CRC collection using the consensus classification system (Guinney et al., 2015). Fig. S2 illustrates control experiments performed for the lineage tracing approach. Fig. S3 shows the immunofluorescence patterns of β-catenin and Cdx2 in serial sections of mixed tumors. Table S1 provides the list of genes differentially expressed between the cecal lesions of $AhCre^{ERT}::Cdx2^{f/f}$ mice and the normal cecum (sheet 1) and lists of selected panels of genes selected from this list (intestinal/gastric markers, stem cell markers, extracellular matrix components, and cytokines, respectively; sheets 2–5). Table S2 provides the list of genes differentially expressed between cecal mixed tumors of $Apc^{+/\Delta 14}::AhCre^{ERT}::Cdx2^{f/f}$ mice and cecal metaplastic-type lesions of $AhCre^{ERT}::Cdx2^{f/f}$ mice (sheet 1) and between small intestinal mixed tumors of $Apc^{+/\Delta 14}::AhCre^{ERT}::Cdx2^{f/f}$ mice and small intestinal adenoma of $Apc^{+/\Delta 14}$ mice (sheet 2).

ACKNOWLEDGMENTS

We thank Prof. M.P. Chenard for help in pathohistology evaluation, Prof. D.J. Winton (Cancer Research UK, Cambridge, England, UK) for the $AhCre^{ERT}$ mice, Dr. C. Perret (Inserm U1016, Institut Cochin, Paris) for the $Apc^{+/\Delta 14}$ mice, Dr. C. Tomaseto (Inserm U1258, IGBMC, Illkirch) for the anti-Tff1 and -Tff2 antibodies, and Dr. A. De Reynes (Cartes d'Identité des Tumeurs Program, Ligue Contre le Cancer, Paris, France) for discussions.

This work was supported by the Ligue Contre le Cancer du Haut-Rhin (France), the Fondation ARC pour la Recherche sur le Cancer (France; PGA120140200834), and the Institut National du Cancer (INCa2014-178). C. Balbinot was funded by the Ministère de l'Enseignement Supérieur et de la Recherche (France) and the Ligue Contre le Cancer.

The authors declare no competing financial interests.

Author contributions: C. Balbinot, F. Beck, J. Deschamps, J.-N. Freund, and I. Duluc conceived and designed the study. C. Balbinot, O. Armant, N. Elarouci, L. Marisa, E. Martin, E. De Clara, A. Onea, J.-N. Freund, and I. Duluc contributed to data acquisition, analysis, and interpretation. C. Balbinot, F. Beck, J.-N. Freund, and I. Duluc wrote the manuscript.

Submitted: 23 May 2017

Revised: 13 November 2017

Accepted: 18 January 2018

REFERENCES

Anders, S., P.T. Pyl, and W. Huber. 2015. HTSeq—A Python framework to work with high-throughput sequencing data. *Bioinformatics.* 31:166–169. https://doi.org/10.1093/bioinformatics/btu638

Andoniadou, C.L., D. Matsushima, S.N. Mousavy Gharavy, M. Signore, A.I. Mackintosh, M. Schaeffer, C. Gaston-Massuet, P. Mollard, T.S. Jacques, P. Le Tissier, et al. 2013. Sox2(+) stem/progenitor cells in the adult mouse pituitary support organ homeostasis and have tumor-inducing potential. *Cell Stem Cell.* 13:433–445. https://doi.org/10.1016/j.stem.2013.07.004

Aoki, K., Y. Tamai, S. Horiike, M. Oshima, and M.M. Taketo. 2003. Colonic polyposis caused by mTOR-mediated chromosomal instability in Apc+/Delta716 Cdx2+/- compound mutant mice. *Nat. Genet.* 35:323–330. https://doi.org/10.1038/ng1265

Bae, J.M., T.H. Lee, N.-Y. Cho, T.-Y. Kim, and G.H. Kang. 2015. Loss of CDX2 expression is associated with poor prognosis in colorectal cancer

patients. *World J. Gastroenterol.* 21:1457–1467. https://doi.org/10.3748/wjg.v21.i5.1457

Bahri, R., I.S. Pateras, O. D'Orlando, D.A. Goyeneche-Patino, M. Campbell, J.K. Polansky, H. Sandig, M. Papaioannou, K. Evangelou, P.G. Foukas, et al. 2015. IL-15 suppresses colitis-associated colon carcinogenesis by inducing antitumor immunity. *OncoImmunology.* 4:e1002721. https://doi.org/10.1080/2162402X.2014.1002721

Balbinot, C., M. Vanier, O. Armant, A. Nair, J. Penichon, C. Soret, E. Martin, T. Saandi, J.-M. Reimund, J. Deschamps, et al. 2017. Fine-tuning and autoregulation of the intestinal determinant and tumor suppressor homeobox gene CDX2 by alternative splicing. *Cell Death Differ.* 24:2173–2186. https://doi.org/10.1038/cdd.2017.140

Barker, N., R.A. Ridgway, J.H. van Es, M. van de Wetering, H. Begthel, M. van den Born, E. Danenberg, A.R. Clarke, O.J. Sansom, and H. Clevers. 2009. Crypt stem cells as the cells-of-origin of intestinal cancer. *Nature.* 457:608–611. https://doi.org/10.1038/nature07602

Bastide, P., C. Darido, J. Pannequin, R. Kist, S. Robine, C. Marty-Double, F. Bibeau, G. Scherer, D. Joubert, F. Hollande, et al. 2007. Sox9 regulates cell proliferation and is required for Paneth cell differentiation in the intestinal epithelium. *J. Cell Biol.* 178:635–648. https://doi.org/10.1083/jcb.200704152

Becht, E., A. de Reyniès, N.A. Giraldo, C. Pilati, B. Buttard, L. Lacroix, J. Selves, C. Sautès-Fridman, P. Laurent-Puig, and W.H. Fridman. 2016. Immune and stromal classification of colorectal cancer is associated with molecular subtypes and relevant for precision immunotherapy. *Clin. Cancer Res.* 22:4057–4066. https://doi.org/10.1158/1078-0432.CCR-15-2879

Beck, F., K. Chawengsaksophak, P. Waring, R.J. Playford, and J.B. Furness. 1999. Reprogramming of intestinal differentiation and intercalary regeneration in Cdx2 mutant mice. *Proc. Natl. Acad. Sci. USA.* 96:7318–7323. https://doi.org/10.1073/pnas.96.13.7318

Bonhomme, C., I. Duluc, E. Martin, K. Chawengsaksophak, M.-P. Chenard, M. Kedinger, F. Beck, J.-N. Freund, and C. Domon-Dell. 2003. The Cdx2 homeobox gene has a tumour suppressor function in the distal colon in addition to a homeotic role during gut development. *Gut.* 52:1465–1471. https://doi.org/10.1136/gut.52.10.1465

Calon, A., I. Gross, B. Lhermitte, E. Martin, F. Beck, B. Duclos, M. Kedinger, I. Duluc, C. Domon-Dell, and J.N. Freund. 2007. Different effects of the Cdx1 and Cdx2 homeobox genes in a murine model of intestinal inflammation. *Gut.* 56:1688–1695. https://doi.org/10.1136/gut.2007.125542

Chun, E., S. Lavoie, M. Michaud, C.A. Gallini, J. Kim, G. Soucy, R. Odze, J.N. Glickman, and W.S. Garrett. 2015. CCL2 promotes colorectal carcinogenesis by enhancing polymorphonuclear myeloid-derived suppressor cell population and function. *Cell Reports.* 12:244–257. https://doi.org/10.1016/j.celrep.2015.06.024

Colnot, S., M. Niwa-Kawakita, G. Hamard, C. Godard, S. Le Plenier, C. Houbron, B. Romagnolo, D. Berrebi, M. Giovannini, and C. Perret. 2004. Colorectal cancers in a new mouse model of familial adenomatous polyposis: Influence of genetic and environmental modifiers. *Lab. Invest.* 84:1619–1630. https://doi.org/10.1038/labinvest.3700180

Dalerba, P., D. Sahoo, S. Paik, X. Guo, G. Yothers, N. Song, N. Wilcox-Fogel, E. Forgó, P.S. Rajendran, S.P. Miranda, et al. 2016. CDX2 as a prognostic biomarker in stage II and stage III colon cancer. *N. Engl. J. Med.* 374:211–222. https://doi.org/10.1056/NEJMoa1506597

De Santa Barbara, P., N. Bonneaud, B. Boizet, M. Desclozeaux, B. Moniot, P. Sudbeck, G. Scherer, F. Poulat, and P. Berta. 1998. Direct interaction of SRY-related protein SOX9 and steroidogenic factor 1 regulates transcription of the human anti-Müllerian hormone gene. *Mol. Cell. Biol.* 18:6653–6665. https://doi.org/10.1128/MCB.18.11.6653

De Sousa E Melo, F., X. Wang, M. Jansen, E. Fessler, A. Trinh, L.P. de Rooij, J.H. de Jong, O.J. de Boer, R. van Leersum, M.F. Bijlsma, et al. 2013. Poor-prognosis colon cancer is defined by a molecularly distinct subtype and develops from serrated precursor lesions. *Nat. Med.* 19:614–618. https://doi.org/10.1038/nm.3174

Egeblad, M., E.S. Nakasone, and Z. Werb. 2010. Tumors as organs: Complex tissues that interface with the entire organism. *Dev. Cell.* 18:884–901. https://doi.org/10.1016/j.devcel.2010.05.012

Gross, I., I. Duluc, T. Benameur, A. Calon, E. Martin, T. Brabletz, M. Kedinger, C. Domon-Dell, and J.-N. Freund. 2008. The intestine-specific homeobox gene Cdx2 decreases mobility and antagonizes dissemination of colon cancer cells. *Oncogene.* 27:107–115. https://doi.org/10.1038/sj.onc.1210601

Guinney, J., R. Dienstmann, X. Wang, A. de Reyniès, A. Schlicker, C. Soneson, L. Marisa, P. Roepman, G. Nyamundanda, P. Angelino, et al. 2015. The consensus molecular subtypes of colorectal cancer. *Nat. Med.* 21:1350–1356. https://doi.org/10.1038/nm.3967

Hryniuk, A., S. Grainger, J.G.A. Savory, and D. Lohnes. 2014. Cdx1 and Cdx2 function as tumor suppressors. *J. Biol. Chem.* 289:33343–33354. https://doi.org/10.1074/jbc.M114.583823

Ireland, H., R. Kemp, C. Houghton, L. Howard, A.R. Clarke, O.J. Sansom, and D.J. Winton. 2004. Inducible Cre-mediated control of gene expression in the murine gastrointestinal tract: effect of loss of beta-catenin. *Gastroenterology.* 126:1236–1246. https://doi.org/10.1053/j.gastro.2004.03.020

Karam, S.M., C. Tomasetto, and M.-C. Rio. 2004. Trefoil factor 1 is required for the commitment programme of mouse oxyntic epithelial progenitors. *Gut.* 53:1408–1415. https://doi.org/10.1136/gut.2003.031963

Kim, J.H., K.-J. Kim, Y.-Y. Rhee, J.M. Bae, N.-Y. Cho, H.S. Lee, and G.H. Kang. 2015. Gastric-type expression signature in serrated pathway-associated colorectal tumors. *Hum. Pathol.* 46:643–656. https://doi.org/10.1016/j.humpath.2015.01.003

Liu, W., H. Li, S.-H. Hong, G.P. Piszczek, W. Chen, and G.P. Rodgers. 2016. Olfactomedin 4 deletion induces colon adenocarcinoma in ApcMin/+ mice. *Oncogene.* 35:5237–5247. https://doi.org/10.1038/onc.2016.58

Love, M.I., W. Huber, and S. Anders. 2014. Moderated estimation of fold change and dispersion for RNA-seq data with DESeq2. *Genome Biol.* 15:550. https://doi.org/10.1186/s13059-014-0550-8

Lu, P., V.M. Weaver, and Z. Werb. 2012. The extracellular matrix: A dynamic niche in cancer progression. *J. Cell Biol.* 196:395–406. https://doi.org/10.1083/jcb.201102147

Lujambio, A., L. Akkari, J. Simon, D. Grace, D.F. Tschaharganeh, J.E. Bolden, Z. Zhao, V. Thapar, J.A. Joyce, V. Krizhanovsky, and S.W. Lowe. 2013. Non-cell-autonomous tumor suppression by p53. *Cell.* 153:449–460. https://doi.org/10.1016/j.cell.2013.03.020

Marisa, L., A. de Reyniès, A. Duval, J. Selves, M.P. Gaub, L. Vescovo, M.-C. Etienne-Grimaldi, R. Schiappa, D. Guenot, M. Ayadi, et al. 2013. Gene expression classification of colon cancer into molecular subtypes: Characterization, validation, and prognostic value. *PLoS Med.* 10:e1001453. https://doi.org/10.1371/journal.pmed.1001453

Marusyk, A., D.P. Tabassum, P.M. Altrock, V. Almendro, F. Michor, and K. Polyak. 2014. Non-cell-autonomous driving of tumour growth supports sub-clonal heterogeneity. *Nature.* 514:54–58. https://doi.org/10.1038/nature13556

Matsuda, M., K. Sentani, T. Noguchi, T. Hinoi, M. Okajima, K. Matsusaki, N. Sakamoto, K. Anami, Y. Naito, N. Oue, and W. Yasui. 2010. Immunohistochemical analysis of colorectal cancer with gastric phenotype: Claudin-18 is associated with poor prognosis. *Pathol. Int.* 60:673–680. https://doi.org/10.1111/j.1440-1827.2010.02587.x

Mescher, M., P. Jeong, S.K. Knapp, M. Rübsam, M. Saynisch, M. Kranen, J. Landsberg, M. Schlaak, C. Mauch, T. Tüting, et al. 2017. The epidermal polarity protein Par3 is a non-cell autonomous suppressor of malignant melanoma. *J. Exp. Med.* 214:339–358. https://doi.org/10.1084/jem.20160596

Muñoz, J., D.E. Stange, A.G. Schepers, M. van de Wetering, B.-K. Koo, S. Itzkovitz, R. Volckmann, K.S. Kung, J. Koster, S. Radulescu, et al. 2012. The Lgr5 intestinal stem cell signature: Robust expression of proposed quiescent '+4' cell markers. *EMBO J.* 31:3079–3091. https://doi.org/10.1038/emboj.2012.166

Platet, N., I. Hinkel, L. Richert, D. Murdamoothoo, A. Moufok-Sadoun, M. Vanier, P. Lavalle, C. Gaiddon, D. Vautier, J.-N. Freund, and I. Gross. 2017. The tumor suppressor CDX2 opposes pro-metastatic biomechanical modifications of colon cancer cells through organization of the actin cytoskeleton. *Cancer Lett.* 386:57–64. https://doi.org/10.1016/j.canlet.2016.10.040

Prévostel, C., C. Rammah-Bouazza, H. Trauchessec, L. Canterel-Thouennon, M. Busson, M. Ychou, and P. Blache. 2016. SOX9 is an atypical intestinal tumor suppressor controlling the oncogenic Wnt/ß-catenin signaling. *Oncotarget.* 7:82228–82243. https://doi.org/10.18632/oncotarget.10573

Putoczki, T.L., S. Thiem, A. Loving, R.A. Busuttil, N.J. Wilson, P.K. Ziegler, P.M. Nguyen, A. Preaudet, R. Farid, K.M. Edwards, et al. 2013. Interleukin-11 is the dominant IL-6 family cytokine during gastrointestinal tumorigenesis and can be targeted therapeutically. *Cancer Cell.* 24:257–271. https://doi.org/10.1016/j.ccr.2013.06.017

Renouf, B., C. Soret, T. Saandi, F. Delalande, E. Martin, M. Vanier, I. Duluc, I. Gross, J.-N. Freund, and C. Domon-Dell. 2012. Cdx2 homeoprotein inhibits non-homologous end joining in colon cancer but not in leukemia cells. *Nucleic Acids Res.* 40:3456–3469. https://doi.org/10.1093/nar/gkr1242

Sakamoto, N., Y. Feng, C. Stolfi, Y. Kurosu, M. Green, J. Lin, M.E. Green, K. Sentani, W. Yasui, M. McMahon, et al. 2017. BRAFV600E cooperates with CDX2 inactivation to promote serrated colorectal tumorigenesis. *eLife.* 6:e20331. https://doi.org/10.7554/eLife.20331

Salcedo, R., A. Worschech, M. Cardone, Y. Jones, Z. Gyulai, R.-M. Dai, E. Wang, W. Ma, D. Haines, C. O'hUigin, et al. 2010. MyD88-mediated signaling prevents development of adenocarcinomas of the colon: Role of interleukin 18. *J. Exp. Med.* 207:1625–1636. https://doi.org/10.1084/jem.20100199

Schwitalla, S., A.A. Fingerle, P. Cammareri, T. Nebelsiek, S.I. Göktuna, P.K. Ziegler, O. Canli, J. Heijmans, D.J. Huels, G. Moreaux, et al. 2013. Intestinal tumorigenesis initiated by dedifferentiation and acquisition of stem-cell-like properties. *Cell.* 152:25–38. https://doi.org/10.1016/j.cell.2012.12.012

Sentani, K., N. Sakamoto, F. Shimamoto, K. Anami, N. Oue, and W. Yasui. 2013. Expression of olfactomedin 4 and claudin-18 in serrated neoplasia of the colorectum: A characteristic pattern is associated with sessile serrated lesion. *Histopathology.* 62:1018–1027. https://doi.org/10.1111/his.12099

Shaked, H., L.J. Hofseth, A. Chumanevich, A.A. Chumanevich, J. Wang, Y. Wang, K. Taniguchi, M. Guma, S. Shenouda, H. Clevers, et al. 2012. Chronic epithelial NF-κB activation accelerates APC loss and intestinal tumor initiation through iNOS up-regulation. *Proc. Natl. Acad. Sci. USA.* 109:14007–14012. https://doi.org/10.1073/pnas.1211509109

Shih, I.M., T.L. Wang, G. Traverso, K. Romans, S.R. Hamilton, S. Ben-Sasson, K.W. Kinzler, and B. Vogelstein. 2001. Top-down morphogenesis of colorectal tumors. *Proc. Natl. Acad. Sci. USA.* 98:2640–2645. https://doi.org/10.1073/pnas.051629398

Simmini, S., M. Bialecka, M. Huch, L. Kester, M. van de Wetering, T. Sato, F. Beck, A. van Oudenaarden, H. Clevers, and J. Deschamps. 2014. Transformation of intestinal stem cells into gastric stem cells on loss of transcription factor Cdx2. *Nat. Commun.* 5:5728. https://doi.org/10.1038/ncomms6728

Stringer, E.J., C.A. Pritchard, and F. Beck. 2008. Cdx2 initiates histodifferentiation of the midgut endoderm. *FEBS Lett.* 582:2555–2560. https://doi.org/10.1016/j.febslet.2008.06.024

Stringer, E.J., I. Duluc, T. Saandi, I. Davidson, M. Bialecka, T. Sato, N. Barker, H. Clevers, C.A. Pritchard, D.J. Winton, et al. 2012. Cdx2 determines the fate of postnatal intestinal endoderm. *Development.* 139:465–474. https://doi.org/10.1242/dev.070722

Tong, K., O. Pellón-Cárdenas, V.R. Sirihorachai, B.N. Warder, O.A. Kothari, A.O. Perekatt, E.E. Fokas, R.L. Fullem, A. Zhou, J.K. Thackray, et al. 2017. Degree of tissue differentiation dictates susceptibility to BRAF-driven colorectal cancer. *Cell Reports.* 21:3833–3845. https://doi.org/10.1016/j.celrep.2017.11.104

Trapnell, C., L. Pachter, and S.L. Salzberg. 2009. TopHat: Discovering splice junctions with RNA-Seq. *Bioinformatics.* 25:1105–1111. https://doi.org/10.1093/bioinformatics/btp120

Verzi, M.P., H. Shin, H.H. He, R. Sulahian, C.A. Meyer, R.K. Montgomery, J.C. Fleet, M. Brown, X.S. Liu, and R.A. Shivdasani. 2010. Differentiation-specific histone modifications reveal dynamic chromatin interactions and partners for the intestinal transcription factor CDX2. *Dev. Cell.* 19:713–726. https://doi.org/10.1016/j.devcel.2010.10.006

Verzi, M.P., H. Shin, L.-L. Ho, X.S. Liu, and R.A. Shivdasani. 2011. Essential and redundant functions of caudal family proteins in activating adult intestinal genes. *Mol. Cell. Biol.* 31:2026–2039. https://doi.org/10.1128/MCB.01250-10

Zhang, Y., J. Gao, X. Wang, S. Deng, H. Ye, W. Guan, M. Wu, S. Zhu, Y. Yu, and W. Han. 2015. CXCL4 mediates tumor regrowth after chemotherapy by suppression of antitumor immunity. *Cancer Biol. Ther.* 16:1775–1783. https://doi.org/10.1080/15384047.2015.1095404